

Nuclear Argonaute protein NRDE-3 switches small RNA binding partners during embryogenesis coincident with the formation of SIMR granules

Shihui Chen, Carolyn M Phillips 

Department of Biological Sciences, University of Southern California, Los Angeles, CA 90089, United States

 https://en.wikipedia.org/wiki/Open_access
 Copyright information

eLife Assessment

The study by Chen and Phillips provides evidence for a dynamic switch in the small RNA repertoire of the Argonaute protein NRDE-3 during embryogenesis in *C. elegans*. The work is supported by **solid** experimental data, although some conclusions regarding the functional role of specific RNA granules remain uncertain. Nevertheless, this study offers **valuable** insights into RNA regulation and developmental biology, with broader implications for understanding small RNA pathways in other systems.

<https://doi.org/10.7554/eLife.102226.1.sa3>

Abstract

RNA interference (RNAi) is a conserved gene regulation mechanism that utilizes the Argonaute protein and their associated small RNAs to exert regulatory function on complementary transcripts. While the majority of germline-expressed RNAi pathway components reside in perinuclear germ granules, it is unknown whether and how RNAi pathways are spatially organized in other cell types. Here we find that the small RNA biogenesis machinery is spatially and temporally organized during embryogenesis. Specifically, the RNAi factor, SIMR-1, forms visible concentrates during mid-embryogenesis that contain an RNA-dependent RNA polymerase, a poly-UG polymerase, and the unloaded nuclear Argonaute protein, NRDE-3. Further, we observe that many other RNAi factors form foci in embryonic cells distinct from SIMR granules, including the Argonaute protein CSR-1, underscoring a potential role for cytoplasmic concentrates of RNAi factors to promote gene regulation in embryos. Curiously, coincident with the appearance of the “SIMR granules”, the small RNAs bound to NRDE-3 switch from predominantly CSR-class 22G-RNAs to ERGO-dependent 22G-RNAs. Thus, our study defines two separable roles for NRDE-3, targeting germline-expressed genes during early embryogenesis and switching later in embryogenesis to repress recently duplicated genes and retrotransposons in somatic cells, highlighting the plasticity of Argonaute proteins and the need for more precise temporal characterization of Argonaute-small RNA interactions.

Introduction

Precise gene expression is essential for organisms at all developmental stages. Small RNAs and their partners, the Argonaute (AGO) proteins, play an important role in regulating gene expression by targeting and silencing complementary nucleic acid sequences. This small RNA-mediated gene silencing process is known as RNA interference (RNAi) (Fire et al. 1998 [\[1\]](#)). The nematode *Caenorhabditis elegans*, distinguished by its expanded Argonaute family and intricate RNAi pathway, is a well-established model organism to study the RNAi pathway. *C. elegans* has 19 functional Argonaute proteins and various classes of small RNAs (Yigit et al. 2006 [\[2\]](#); Seroussi et al. 2023 [\[3\]](#)), which is greatly expanded compared to 8 Argonaute proteins in mammals, 5 in *Drosophila melanogaster*, and 1 in *Schizosaccharomyces pombe* (Höck and Meister 2008 [\[4\]](#)). This expansion of the Argonaute family in nematodes may be linked to the diversity of habitats in which nematodes reside and environmental cues to which they must respond. First, RNAi has been well-studied in plants for its role as an antiviral defense mechanism (Ding et al. 2004 [\[5\]](#)); and like plants, worms lack an adaptive immune system, making the RNAi system a primary means to respond to viral intruders (Félix et al. 2011 [\[6\]](#); Ashe et al. 2013 [\[7\]](#); Sarkies and Miska 2013 [\[8\]](#)). Second, nematodes have a specialized nucleic acid transporter required for the uptake of double-strand (ds)RNA from the intestinal lumen (McEwan et al. 2012 [\[9\]](#); Winston et al. 2007 [\[10\]](#)), indicating that environmental sensing mediated by ingested dsRNA is an important aspect of nematode physiology (Sarkies and Miska 2013 [\[8\]](#)). Lastly, it has been proposed that Ago diversity and rapid evolution could be linked to the environmental plasticity of nematodes, including the capacity for parasitism and challenges of invading and colonizing a host (Buck and Blaxter 2013 [\[11\]](#)). Regardless of the evolutionary origin for the expansion of RNAi pathway proteins in nematodes, these pathways are not only important for a response to the environment, but are essential for the regulation of thousands of endogenous genes. Therefore, untangling the details of RNA silencing in *C. elegans* will shed light on the mechanisms of small RNA-mediated gene regulation in *C. elegans* and other organisms.

Argonaute proteins can be subdivided into three clades. Proteins are grouped into the AGO and PIWI clades based on their similarity to *Arabidopsis thaliana* AGO1 and *Drosophila melanogaster* PIWI, respectively. The third, WAGO, clade represents a nematode-specific expansion of the Argonaute protein family (Yigit et al. 2006 [\[2\]](#)). While small RNAs bound by the AGO- and PIWI-clade Argonaute proteins tend to be processed from longer, precursor transcripts, the WAGO-clade Argonaute proteins bind 22-nucleotide, 5'-triphosphorylated small RNAs (22G-RNAs) with which are each de novo synthesized by RNA-dependent RNA polymerases (RdRPs) (Gu et al. 2009 [\[12\]](#); Pak and Fire 2007 [\[13\]](#); Aoki et al. 2007 [\[14\]](#)). However, even within the WAGO clade, each of the 11 Argonaute proteins exhibits specificity for a unique group of 22G-RNAs and exhibits distinct tissue and developmental expression patterns (Seroussi et al. 2023 [\[3\]](#)). For example, WAGO-1 binds 22G-RNAs that target transposons, pseudogenes, and aberrant transcripts, and silences genes post-transcriptionally in the germline cytoplasm (Gu et al. 2009 [\[12\]](#)), while CSR-1 binds 22G-RNAs targeting germline-expressed genes, functioning to clear maternal mRNA in early embryos while licensing and tuning gene expression in the adult germline (Quarato et al. 2021 [\[15\]](#); Gu et al. 2009 [\[12\]](#); Claycomb et al. 2009 [\[16\]](#)). Other WAGO Argonautes, such as SAGO-1 and SAGO-2, function exclusively in somatic cells and play roles in regulating endogenous genes, exogenous RNAi, and immunity (Seroussi et al. 2023 [\[3\]](#)). Unique amongst the WAGO Argonautes for their nuclear localization are HRDE-1 and NRDE-3, which are thought to silence genes co-transcriptionally in germline and soma respectively, and are required for the inheritance of RNA silencing signals from parents to offspring (Buckley et al. 2012 [\[17\]](#); Guang et al. 2008 [\[18\]](#)). Despite extensive characterization of the *C. elegans* Argonaute proteins, we still know little about the factors that promote the spatiotemporal expression of each Argonaute protein and the mechanisms that promote Argonaute-small RNA binding specificity. Furthermore, most Argonaute-small RNA

sequencing experiments have been performed at a single time point, usually in adult *C. elegans*, meaning that we have little understanding as to how the RNA targets of each Argonaute protein change across development.

In the *C. elegans* germline, many of the RNAi components, including Argonaute proteins, RdRPs, and other small RNA processing machinery, localize within phase-separated germ granules. Often, proteins acting in different functional branches of the RNAi pathway seem to reside in separate compartments of the germ granules, suggesting that there are specialized areas within the germ granules where distinct molecular reactions occur. Presently, four sub-compartments of the germ granule have been identified in *C. elegans*: P granules, *Mutator* foci, Z granules, and SIMR foci (Brangwynne et al. 2009 [\[1\]](#); Phillips et al. 2012 [\[2\]](#); Wan et al. 2018 [\[3\]](#); Manage et al. 2020 [\[4\]](#)). These germ granule compartments are situated at the cytoplasmic side of the nucleus, proximal to nuclear pores. However, the mechanisms governing their spatial organization remain unknown. Moreover, with the majority of studies focusing on mechanisms of RNA silencing and germ granule organization in the germline, there is limited understanding of how each of these germ granule compartments assembles and functions in embryos. It has been observed that in *C. elegans* embryogenesis, the primordial germline cell P4 divides into Z2 and Z3 progenitor germ cells (PGCs) at around the 100-cell stage, coinciding with the demixing of Z granules from P granules, the appearance of *Mutator* foci and SIMR foci, and the initiation of germ cell transcription (Updike and Strome 2010 [\[5\]](#); Uebel et al. 2021 [\[6\]](#); Wan et al. 2018 [\[3\]](#); Seydoux and Dunn 1997 [\[7\]](#)). Together, the assembly of this more complex germ granule organization coinciding with a burst of transcription from the germ cells, may indicate that these multi-compartment structures are necessary to monitor the newly-synthesized germline transcripts. Yet even these limited studies of RNAi pathway factors in embryos fail to address a role for ribonucleoprotein granules in RNA silencing in the soma.

Here, we discovered that SIMR-1, the founding component of the germline SIMR foci, is also found in cytoplasmic granules in the somatic cells of *C. elegans* embryos. These embryonic SIMR granules additionally contain factors involved in 22G-RNA amplification and associated with the nuclear Argonaute protein, NRDE-3. However, NRDE-3 itself only associates with the SIMR granules when not bound to small RNAs. Strikingly, the SIMR granules exhibit temporal dynamics where they first appear in early embryogenesis (around the 8-cell stage), peak around the 100-cell stage, and have mostly disappeared by the comma stage of embryogenesis. Curiously, these embryonic SIMR granules are by no means the only RNAi-related embryonic granules, as numerous other RNAi factors are found in separate granules in embryos, including components of the CSR pathway, the Argonaute CSR-1 and its RdRP EGO-1. Furthermore, by sequencing the small RNAs bound by NRDE-3 in early and late embryogenesis, we found that the formation of the SIMR granules coincides with a switch in NRDE-3 small RNA targets, from CSR-class 22G-RNAs to ERGO-class 22G-RNAs. Together, our data demonstrates that NRDE-3 has two separate functions, first acting with CSR-1 in early embryogenesis, possibly to transcriptionally silence germline-expressed transcripts in somatic cells, and second acting downstream of ERGO-1 to transcriptionally silence retrotransposons, pseudogenes, and aberrant transcripts. Further, the SIMR granules themselves appear to be sites of NRDE-3-bound 22G-RNA biogenesis and loading and may contribute to the efficiency or specificity of Argonaute-small RNA interactions during embryogenesis.

Results

SIMR-1 and ENRI-2 localize to cytoplasmic granules during embryogenesis

In previous work, we sought to identify proteins that associate with SIMR-1 and ultimately found that SIMR-1 associates with HRDE-2 and the nuclear Argonaute protein, HRDE-1, to promote correct HRDE-1 small RNA binding in germ cells (Chen and Phillips 2024 [\[8\]](#)). In that work, we also

identified another nuclear Argonaute protein, NRDE-3, as an interactor of SIMR-1. To delve further into this potential interaction between SIMR-1 and NRDE-3, we first systematically compiled a list of the protein interactions identified from previous studies for both SIMR-1 and NRDE-3 (**Fig. 1A**). Interestingly, the HRDE-2 paralog, ENRI-2, had been shown to interact with both SIMR-1 and NRDE-3 in embryos by immunoprecipitation followed by mass spectrometry (IP mass-spec), and another HRDE-2 paralog, ENRI-1, was similarly shown to interact with only NRDE-3 (Lewis et al. 2020). These findings suggest that SIMR-1, NRDE-3, ENRI-2, and possibly ENRI-1 proteins may function together in the somatic nuclear RNAi pathway, analogous to the roles of SIMR-1, HRDE-1, and HRDE-2 in the germline nuclear RNAi pathway.

Here, we first aimed to address whether and where NRDE-3, SIMR-1, ENRI-1, and ENRI-2 colocalize. NRDE-3 has previously been shown to be expressed in the nucleus of most somatic cells (Guang et al. 2008). Until recently, all characterization of NRDE-3 was done using a low-copy, integrated transgenic strain in which the nuclear localization was not visible until the ~30-80-cell stage of development, and it was presumed that this localization reflected the endogenous NRDE-3 localization (Guang et al. 2008; Lewis et al. 2020). However, a more recent study constructed an endogenously-tagged NRDE-3 strain using CRISPR and found that NRDE-3 additionally localizes to the nucleus of oocytes and early embryos (Seroussi et al. 2023, 2022), suggesting that the older, transgenic NRDE-3 construct may be targeted for silencing in germ cells. SIMR-1 is a component of the SIMR foci, a sub-compartment of germ granules, that appears as punctate foci at the periphery of *C. elegans* germ cells starting in embryos through the adult stage (Manage et al. 2020; Uebel et al. 2021). ENRI-1 has been reported to localize to the cytoplasm of oocytes and embryos while ENRI-2 localized to both the nucleus and cytoplasm, varying depending on developmental stage (Lewis et al. 2020). With these four proteins showing distinct localization patterns from one another, it was unclear how these proteins could physically interact.

To investigate where and how these interactions might potentially occur, we chose to initially examine localization of these proteins in the germline of adult *C. elegans* using the endogenously-tagged NRDE-3 strain which is visible starting in late pachytene. As expected based on previous work, NRDE-3 localizes to the nucleus of germ cells, while SIMR-1 is found in the cytoplasm in SIMR foci, a compartment of the germ granule (Supplementary Fig. 1A) (Seroussi et al. 2022, 2023; Manage et al. 2020). Next, we decided to examine NRDE-3 and SIMR-1 localization in embryos, carefully dividing the embryos into distinct developmental stages, from 4-cell to comma stage. As expected, we found that NRDE-3 is consistently localized to the nucleus in all embryonic stages (**Fig. 1B**). Interestingly, we observed that SIMR-1 forms granules in the cytoplasm of somatic cells during some embryonic stages (**Fig. 1B**). By quantifying the total number of granules per embryo across embryonic development, we found that the SIMR-1 granules first appear around the 8-cell stage and reach a peak at approximately the 100-cell stage, coinciding with the division of the germline precursor cell P₄ into the primordial germ cells Z₂ and Z₃ (Wang and Seydoux 2013). Subsequently, the number of SIMR-1 granules decreases, and in late embryos, SIMR-1 localizes primarily to the germ granules surrounding the two germ cells, as previously observed (Uebel et al. 2021) (**Fig. 1B,C**). We had previously shown that the Tudor domain of SIMR-1 was important for its assembly into germline SIMR foci. Therefore, we next explored the requirement for the Tudor domain in assembling SIMR-1 cytoplasmic granules in embryos (Manage et al. 2020). We found that the Tudor domain mutant, SIMR-1(R159C), fails to assemble in cytoplasmic granules in the embryos (Supplementary Fig. 1B), indicating that, similar to germline SIMR foci, the Tudor domain is also required for assembly of the cytoplasmic SIMR granules in embryos.

We next focused on ENRI-1 and ENRI-2 and observed that ENRI-2 shows similar cytoplasmic granule localization and colocalizes with SIMR-1 in embryos, but it does not localize to the germ granules in Z₂ and Z₃, suggesting that the activity of ENRI-2 is restricted to somatic cells (**Fig. 1B**). Finally, we examined the localization N-terminal tagged 2xTy1::GFP::ENRI-1, and found that we could not detect any specific localization in either nuclei or cytoplasmic granules

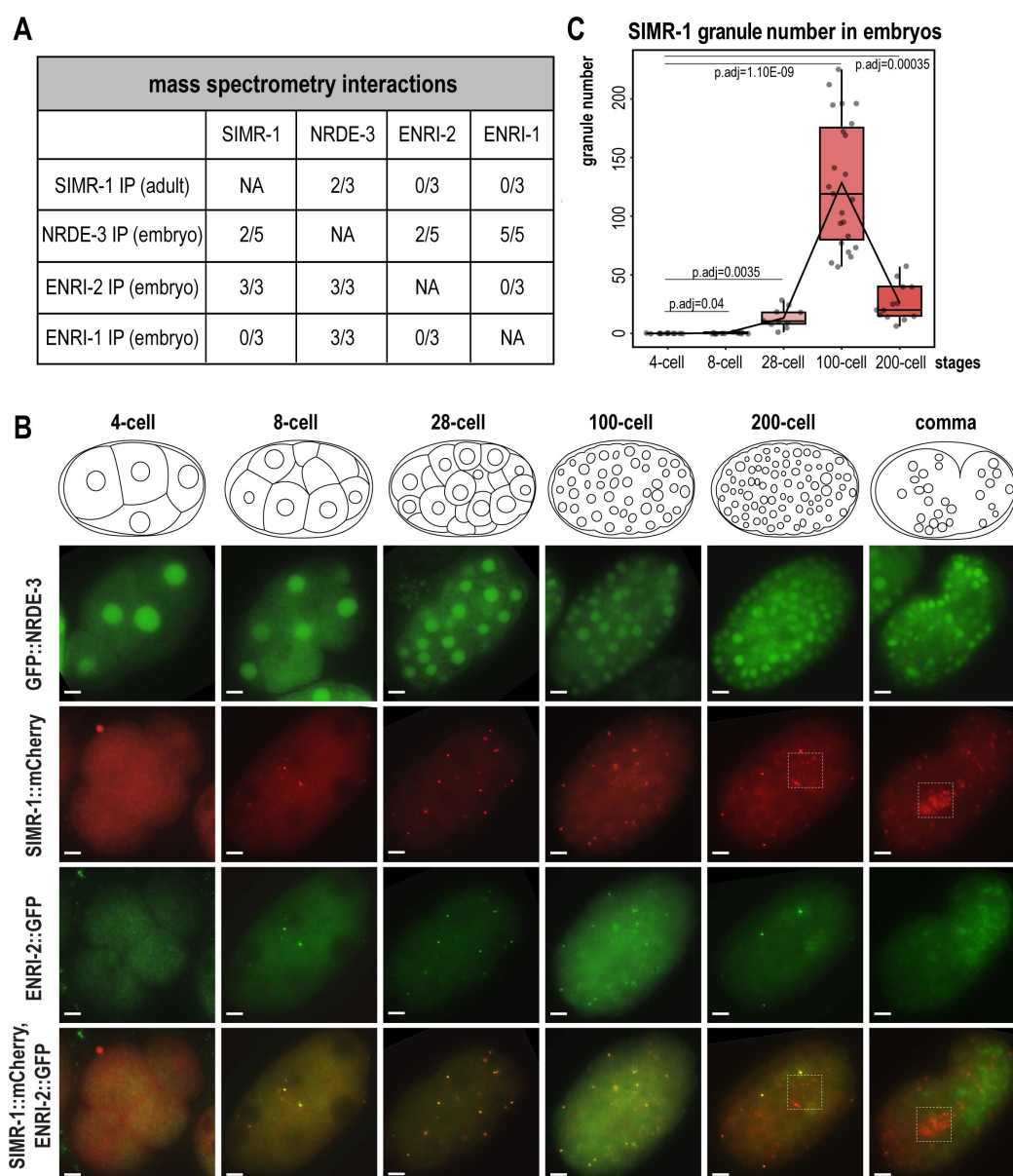


Figure 1.

SIMR-1 and ENRI-2 colocalize at somatic granules in embryos.

A. Summary of IP-mass spectrometry interactions detected between NRDE-3, ENRI-2, ENRI-1, and SIMR-1 from previously published studies (Chen and Phillips, 2024 [DOI](#), Lewis *et al.*, 2021). The number of replicates from which the interaction was detected relative to the total number of replicates performed is indicated.

B. Live imaging of GFP::3xFLAG::NRDE-3 and SIMR-1::mCherry::2xHA; ENRI-2::2xTy1::GFP embryos at different stages (4-cell, 8-cell, 28-cell, 100-cell, 200-cell, and comma). Boxes identify the location of Z₂ and Z₃ primordial germ cells, showing that SIMR-1 is present in germ granules while ENRI-2 is not. At least five individual embryos were imaged for each genotype and stage. Scale bars, 5 μ m.

C. Box plot of SIMR-1::mCherry::2xHA granule number quantification at different embryonic stages (4-cell, 8-cell, 28-cell, 100-cell, and 200-cell). At least ten individual embryos at each stage were used for quantification. Each dot represents an individual embryo, and all data points are shown. Bolded midline indicates median value, box indicates the first and third quartiles, and whiskers represent the most extreme data points within 1.5 times the interquartile range. Lines connect the mean granule number for each stage, illustrating the change in number of SIMR-1 granules across the developmental stages of the embryo. Two-tailed t-tests were performed to determine statistical significance and p-values were adjusted for multiple comparisons. See Materials and Methods for a detailed description of quantification methods.

(Supplementary Fig. 1C) (Lewis et al. 2020). Consequently, we constructed a new strain with C terminal tagged ENRI-1::mCherry::2xHA and confirmed the presence of full-length ENRI-1 protein with Western Blot (Supplementary Fig. 1D). Nonetheless, we could not detect any ENRI-1 localization in embryos with our newly generated strain (Supplementary Fig. 1C). These results are consistent with the fact that ENRI-1 does not interact directly with either SIMR-1 or ENRI-2 by immunoprecipitation (Fig. 1A) (Lewis et al. 2020). Altogether, these data indicate that SIMR-1 and ENRI-2 colocalize at cytoplasmic granules in the somatic cells of embryos and suggest that ENRI-2 and SIMR-1 may function together at these sites. In contrast, NRDE-3 is spatially separated in the nucleus and no clear expression pattern was observed for ENRI-1.

Unloaded NRDE-3 associates with SIMR-1 in cytoplasmic granules

Next, to determine whether SIMR-1 and ENRI-2 are required for NRDE-3 localization, we introduced the *simr-1* mutant, *enri-2* mutant, *enri-1* mutant, and *enri-1; enri-2* double mutant in the endogenously tagged GFP::3xFLAG::NRDE-3 strain, and examined NRDE-3 localization across embryonic developmental stages. We observed no changes in NRDE-3 expression or nuclear localization in any of the mutants examined at any developmental stage (Supplementary Fig. 2A).

In previous work, we demonstrated that the germline nuclear Argonaute protein HRDE-1 loses nuclear localization and associates in the cytoplasm with the SIMR compartment of germ granules when it is unable to bind small RNAs (Chen and Phillips 2024). Additionally, ENRI-2 interacts more strongly with NRDE-3 in an *eri-1* mutant background compared to wild-type (Lewis et al. 2020), suggesting that the interaction occurs when NRDE-3 does not bind small RNAs. Localization of unloaded NRDE-3 has been examined in the seam cells of L3 stage animals, where, like HRDE-1, it loses nuclear localization and becomes restricted to the cytoplasm (Guang et al. 2008). Therefore, we next sought to examine the localization of NRDE-3 when it is unbound to small RNA in embryos and germline. First, we aimed to deplete the preferred small RNA binding partners of NRDE-3. NRDE-3 has previously been shown to bind secondary 22G-RNAs downstream of ERGO-class 26G-RNAs, dependent on ERI-1, which is required for 26G-RNA biogenesis (Guang et al. 2008; Han et al. 2009; Seroussi et al. 2023), and RDE-3/MUT-2, which is a component of the *Mutator* complex and necessary for 22G-RNA production (Chen et al. 2005; Phillips et al. 2012, 2014). Therefore, we introduced an *eri-1* mutant and a *rde-3/mut-2* mutant into the endogenously GFP-tagged NRDE-3 background. We observed that NRDE-3 associates with somatic granules with a similar spatiotemporal pattern to SIMR-1 and ENRI-2, peaking around the 100-cell stage, although the total number of granules per embryo is lower for NRDE-3 granules in the *eri-1* and *rde-3/mut-2* mutant backgrounds compared to SIMR granules (Fig. 2A,B). Next, to fully abolish the small RNA binding capacity of NRDE-3 and to confirm that the observed granule localization was due to the loss of small RNA loading, we introduced mutations to abolish small RNA binding into the GFP-tagged NRDE-3; specifically, residues 687H and 691K in the Mid domain were mutated to alanine, hereafter referred to as NRDE-3(HK-AA) (Ma et al. 2005; Guang et al. 2008; Chen and Phillips 2024). NRDE-3(HK-AA) localizes exclusively to the cytoplasm across embryonic development and in the adult germline, accumulating in somatic granules at 100-cell stage similar to SIMR-1 and ENRI-2 (Fig. 2A). Quantification of the number of NRDE-3 granules per embryo in the NRDE-3(HK-AA) strain shows that the dynamics of NRDE-3 granule appearance and disappearance are similar to that of SIMR-1, where the number of granules increases from early embryos up until about 100-cell stage and then decreases as the embryos progress to later stages of development (Fig. 2C). Overall the total number of NRDE-3(HK-AA) granules quantified per embryo are similar to or modestly higher than SIMR-1 granules (Fig. 1C, Fig. 2B,C). It is also worth noting that despite the similarity in timing of NRDE-3 granule appearance and disappearance in the *eri-1* and *rde-3* mutants compared to the *nrde-3(HK-AA)* mutant, we observed a striking difference in the NRDE-3 localization in early embryos. Specifically, in *eri-1* and *rde-3* mutants, NRDE-3 localizes to the nucleus in early embryos while NRDE-3(HK-AA) localizes exclusively to the cytoplasm (Fig. 2A). Similarly, in the Z2 and Z3 primordial germ cells of late embryos, NRDE-3 is still found in the nucleus in *eri-1* and *rde-3* mutants. In contrast, NRDE-3

localizes exclusively to the cytoplasm in the somatic cells of late embryos of all three mutants. Regardless, these data indicate that NRDE-3 forms granules in the cytoplasm of somatic cells when not associated with a small RNA binding partner.

To determine whether unloaded NRDE-3 localizes to SIMR-1 granules, we examined the localization of SIMR-1 and NRDE-3 together in the *nrde-3(HK-AA)* mutant and *eri-1* mutant backgrounds. We found that SIMR-1 colocalizes perfectly with unloaded NRDE-3 in embryonic granules (**Fig. 2D** [↗](#), Supplementary Fig. 2B). Further, the SIMR-1 granules in the *nrde-3(HK-AA)* mutant background exhibit dynamics similar to the wild-type background (Supplementary Fig. 2C), indicating that *nrde-3(HK-AA)* does not affect the localization of SIMR-1. Interestingly, NRDE-3(HK-AA) does not form granules in germ cells and is instead present exclusively in the cytoplasm, thus it does not colocalize with the SIMR compartment of germ granules (Supplementary Fig. 2D). These results demonstrate that unloaded NRDE-3 associates with SIMR-1 and ENRI-2 in cytoplasmic granules in the somatic cells of *C. elegans* embryos, indicating a potential role for SIMR-1 in the NRDE-3 nuclear RNAi pathway.

SIMR-1 and ENRI-2 recruits unloaded NRDE-3 to cytoplasmic granules

As previously described, unloaded NRDE-3 localizes to cytoplasmic granules in embryos and colocalizes with SIMR-1. Next, we aimed to determine whether SIMR-1 and ENRI-2 are required for the NRDE-3 granule localization. To this end, we introduced a *simr-1* mutant and an *enri-2* mutant into the GFP-tagged NRDE-3(HK-AA) strain and assessed NRDE-3(HK-AA) localization. Strikingly, we found that NRDE-3(HK-AA) granules disappear completely and NRDE-3(HK-AA) is instead found exclusively in the cytoplasm in all cells across all embryonic stages (**Fig. 3A** [↗](#)). Similarly, in a *simr-1; eri-1* double mutant, NRDE-3 granules are absent though NRDE-3 remains in the nucleus in early embryos (**Fig. 3A** [↗](#)), similar to NRDE-3 expression in the *eri-1* single mutant (**Fig. 2A** [↗](#)). These results demonstrate that both SIMR-1 and ENRI-2 are required for the recruitment of NRDE-3 to cytoplasmic granules.

In addition, to assess whether ENRI-1 plays a role in the accumulation of unloaded NRDE-3 in cytoplasmic granules, we introduced an *enri-1* mutant into the GFP-tagged NRDE-3(HK-AA) strain and found that NRDE-3 association with cytoplasmic granules was not disrupted (Supplementary Fig. 3A). We further examined NRDE-3(HK-AA) granule association in the *enri-1; enri-2* double mutant and found it to be fully cytoplasmic, indistinguishable from the *enri-2* single mutant (Supplementary Fig. 3A). While we had already determined that ENRI-1::mCherry did not form visible foci in embryos; to rule out the possibility of partial redundancy between ENRI-1 and ENRI-2, we introduced an *enri-2* mutant into the mCherry-tagged ENRI-1 strain but still unable to detect any distinct ENRI-1 expression (Supplementary Fig. 3B). Lastly, to determine if NRDE-3 recruitment to granules could alter ENRI-1 localization, we introduced the mCherry-tagged ENRI-1 into the GFP-tagged NRDE-3(HK-AA) strain, and still we could not see any granule localization for ENRI-1 (Supplementary Fig. 3C). Therefore, we conclude that ENRI-1 does not function with SIMR-1, ENRI-2, and NRDE-3 at cytoplasmic granules in embryos and we excluded ENRI-1 from further investigation.

To investigate the dependence of SIMR-1 and ENRI-2 on one another, we examined ENRI-2 localization in a *simr-1* mutant and SIMR-1 localization in an *enri-2* mutant. We found that ENRI-2 granules are lost in the *simr-1* mutant, while SIMR-1 granules are still present in the *enri-2* mutant, indicating that SIMR-1 functions upstream of ENRI-2 for granule assembly (**Fig. 3B** [↗](#)). Therefore, we conclude that SIMR-1 and ENRI-2, but not ENRI-1, recruit unloaded NRDE-3 to cytoplasmic granules, with SIMR-1 also acting to recruit ENRI-2.

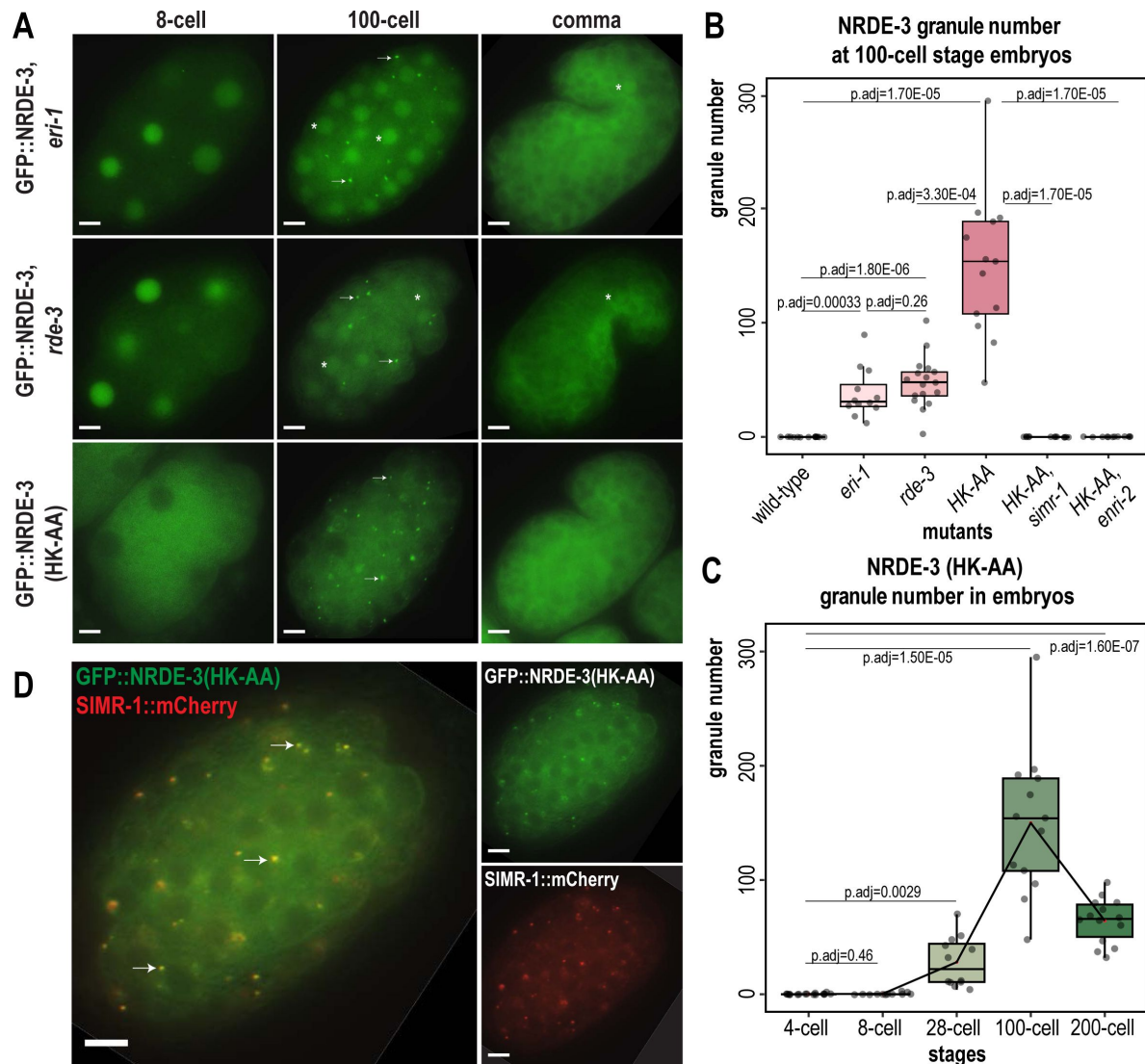


Figure 2.

Unloaded NRDE-3 localizes to cytoplasmic granules with SIMR-1.

A. Live imaging of GFP::3xFLAG::NRDE-3 embryos in *eri-1*, *rde-3*, and *nrde-3*(HK-AA) mutants at 8-cell, 100-cell, and comma stage embryos. At least five individual embryos were imaged for each genotype and stage. Arrows point to granule localization of NRDE-3 in the 100-cell stage. Asterisks highlights the localization of NRDE-3 to the nucleus of the Z2 and Z3 primordial germ cells. Scale bars, 5 μ m.

B. Box plot of GFP::3xFLAG::NRDE-3 granule number quantification in different mutants.

C. Box plot of GFP::3xFLAG::NRDE-3(HK-AA) granule number quantification at different embryonic stages. Lines connect the mean granule number (red dots) for each stage, illustrating the change in change in number of NRDE-3 granules across embryonic development.

D. Live imaging of SIMR-1::mCherry::2xHA; GFP::3xFLAG::NRDE-3(HK-AA) at 100-cell stage. Arrows point to examples of colocalization between SIMR-1 and NRDE-3(HK-AA). At least ten individual embryos were imaged. Scale bars, 5 μ m.

For box plots in B and C, at least twelve individual embryos in each mutant were used for quantification. Each dot represents an individual embryo, and all data points are shown. Bolded midline indicates median value, box indicates the first and third quartiles, and whiskers represent the most extreme data points within 1.5 times the interquartile range. Two-tailed t-tests were performed to determine statistical significance and p-values were adjusted for multiple comparisons. See Materials and Methods for a detailed description of quantification methods.

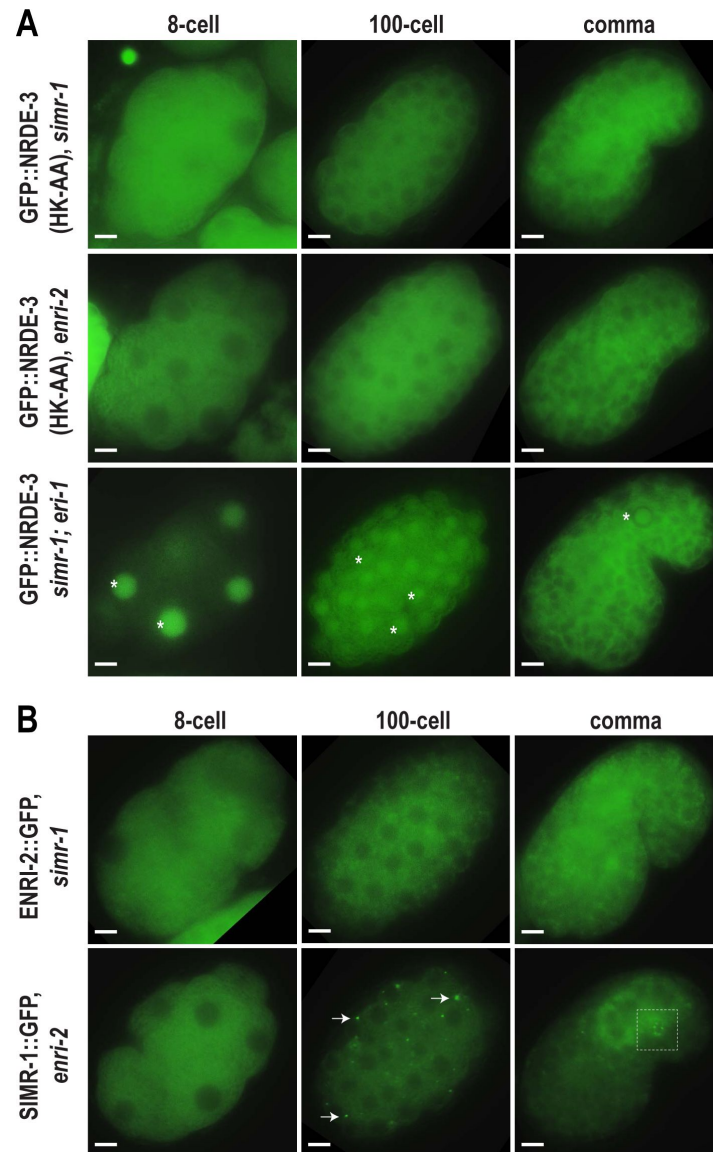


Figure 3.

SIMR-1 recruits ENRI-2 and then NRDE-3 to cytoplasmic granules.

A. Live imaging of GFP::3xFLAG::NRDE-3(HK-AA) embryos in *simr-1* and *eri-2* mutants, and GFP::3xFLAG::NRDE-3 embryos in a *simr-1; eri-1* double mutant at 8-cell, 100-cell, and comma stages. Asterisk marks the nuclear localization of NRDE-3 visible in a primordial germ cell. At least five individual embryos were imaged for each genotype and stage. Scale bars, 5 μ m.

B. Live imaging of ENRI-2::2xTy1::GFP embryos in a *simr-1* mutant and SIMR-1::GFP::3xFLAG embryos in an *eri-2* mutant. At least five individual embryos were imaged for each genotype and stage. Arrows point to examples of cytoplasmic SIMR-1 granules still visible in the *eri-2* mutant. Box surrounds a primordial germ cell displaying germ granule localization of SIMR-1. Scale bars, 5 μ m.

SIMR-1 does not localize to P bodies or other previously identified embryonic granules

A variety of RNA-associated proteins have previously been shown to form granules in *C. elegans* embryos. To determine whether the SIMR-1, ENRI-2, and unloaded NRDE-3 granules that we have observed coincide with a previously identified granule, we examined the colocalization between SIMR-1 and all other embryonic granule-associated proteins that we could identify. It is well known that Processing (P) bodies, the condensates of translationally inactive mRNAs and proteins, localize to cytoplasmic foci of soma in *C. elegans* embryos (Parker and Sheth 2007 [↗](#); Gallo et al. 2008 [↗](#)). To examine if the SIMR-1 cytoplasmic granules are P bodies, we examined the localization of SIMR-1 and CGH-1, a core P body component, using a strain expressing GFP-tagged SIMR-1 and mCherry-tagged CGH-1 (Du et al. 2023 [↗](#)). We found that CGH-1 does not colocalize with SIMR-1 (Supplementary Fig. 4A). CGH-1 also does not colocalize with NRDE-3 cytoplasmic granules in the *eri-1* mutant (Supplementary Fig. 4B). Together, these data indicate that the cytoplasmic SIMR-1 granules found in embryos are not P bodies.

Next, we examined two proteins previously shown to colocalize with SIMR foci in the germ cells of adult animals, RSD-2 and HRDE-2 (Manage et al. 2020 [↗](#); Chen and Phillips 2024 [↗](#)). RSD-2 is a small RNA factor required for the response to low doses of exogenously-introduced double-stranded RNA (Sakaguchi et al. 2014 [↗](#); Han et al. 2008 [↗](#); Tijsterman et al. 2004 [↗](#); Zhang et al. 2012 [↗](#)) and HRDE-2 is a factor critical for RNAi inheritance that promotes correct small RNA loading into the nuclear Argonaute HRDE-1 (Chen and Phillips 2024 [↗](#); Spracklin et al. 2017 [↗](#)). However, we did not observe any granule localization for RSD-2 and HRDE-2 in embryos (Supplementary Fig. 4C,D). In addition, SIMR-1 cytoplasmic granules were not affected by the loss of *hrde-2* (Supplementary Fig. 4E). These results suggest that HRDE-2 and RSD-2 do not function together with SIMR-1, ENRI-2, and NRDE-3 in embryonic granules.

RDE-12 interacts with Argonaute proteins and RNAi-targeted mRNAs, and has also been shown to localize to cytoplasmic granules in the somatic cells of *C. elegans* embryos (Shirayama et al. 2014 [↗](#); Yang et al. 2014 [↗](#)). We next assessed the localization of mCherry-tagged SIMR-1 relative to GFP-tagged RDE-12 and found that they do not colocalize (Supplementary Fig. 4F). RSD-6 is a Tudor domain-containing RNAi factor that partially colocalizes with RDE-12 in the R2 bodies in adult germ cells (Yang et al. 2014 [↗](#); Sakaguchi et al. 2014 [↗](#); Zhang et al. 2012 [↗](#)). We examined the expression of GFP-tagged RSD-6 in embryos and, while we did observe RSD-6 at granules in somatic cells, no colocalization with mCherry-tagged SIMR-1 could be detected (Supplementary Fig. 4G). The RNAi-inheritance factor and defining member of the Z compartment of the germ granule, ZNFX-1, has also been observed in cytoplasmic granules in the somatic cells of embryos (Wan et al. 2018 [↗](#); Ouyang et al. 2019 [↗](#)), however these somatic ZNFX-1 granules also fail to colocalize with SIMR-1 (Supplementary Fig. 4H). Altogether, we found that SIMR-1 fails to localize to any previously characterized embryonic granules. These results further indicate that there are numerous granule-localized proteins in the somatic cells of embryos, such as RDE-12, RSD-6, and ZNFX-1, which may play important roles in the RNA biology of early embryos.

Multiple *Mutator* complex proteins localize to SIMR-1 granules in embryos

Mutator foci localize adjacent to SIMR foci in the adult germline (Manage et al. 2020 [↗](#); Chen and Phillips 2024 [↗](#)), so we next investigated the localization of *Mutator* components in embryos. We first examined *Mutator* foci component RDE-3/MUT-2, a poly(UG) polymerase required for WAGO-class 22G-RNA production (Phillips et al. 2012 [↗](#); Shukla et al. 2020 [↗](#)) and found that GFP-tagged RDE-3 is prominently localized to cytoplasmic granules in embryos that colocalize with SIMR-1 (Fig. 4A [↗](#)). This colocalization led us to the hypothesis that SIMR-1 cytoplasmic granules are sites of WAGO-class 22G-RNA biogenesis. Therefore, we speculated that more small RNA production

machinery might be localized with SIMR-1 at these cytoplasmic granules. We next examined the RNA-dependent-RNA-polymerase (RdRP) RRF-1, which synthesizes WAGO-class 22G-RNAs and localizes to *Mutator* foci in the adult germline (Sijen et al. 2001 [↗](#); Gent et al. 2010 [↗](#); Vasale et al. 2010 [↗](#); Phillips et al. 2012 [↗](#)). As we predicted, RRF-1 also colocalizes with SIMR-1 in somatic granules (**Fig. 4B** [↗](#)), and it fails to localize to somatic granules in the *simr-1* mutant (**Fig. 4C** [↗](#)).

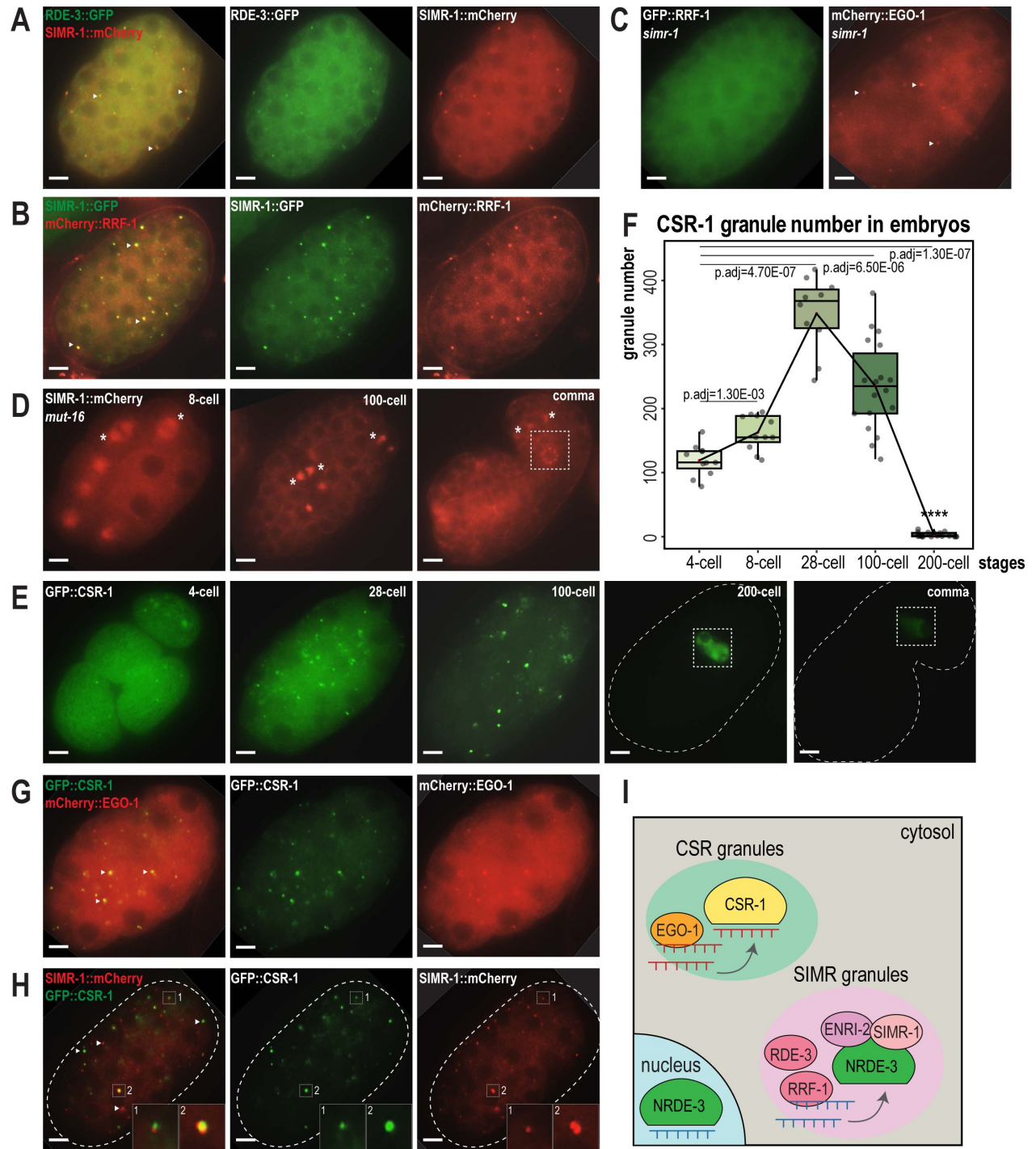


Figure 4.

CSR and WAGO pathway proteins localize to distinct cytoplasmic granules.

A. Live imaging of SIMR-1::mCherry::2xHA; RDE-3::GFP embryo at 100-cell stage, showing that RDE-3 colocalizes with SIMR-1. At least five individual embryos were imaged for each genotype and stage. Arrowheads point to examples of colocalization between SIMR-1 and RDE-3 at cytoplasmic granules. Scale bars, 5 μ m.

B. Live imaging of SIMR-1::GFP::3xFLAG; HA::EGO-1::mCherry::RRF-1 at 100-cell stage embryo, showing that RRF-1 colocalizes with SIMR-1. At least five individual embryos were imaged for each genotype and stage. Arrowheads point to examples of colocalization between SIMR-1 and RRF-1 at cytoplasmic granules. Scale bars, 5 μ m.

C. Live imaging of mCherry::EGO-1::GFP::RRF-1 in a *simr-1* mutant, showing that RRF-1 no longer associates with cytoplasmic granules, while EGO-1 remains associated with granules in the *simr-1* mutant. At least five individual embryos were imaged. Arrowheads point to examples of cytoplasmic EGO-1 granules in a *simr-1* mutant. Scale bars, 5 μ m.

D. Live imaging of SIMR-1::mCherry::2xHA embryos in a *mut-16* mutant at 8-cell, 100-cell, and comma stages. At least five individual embryos were imaged. Asterisks indicate spindle localization of SIMR-1 in a *mut-16* mutant. Box highlights germ granule localization of SIMR-1 in a comma-stage, *mut-16* mutant embryo. Scale bars, 5 μ m.

E. Live imaging of GFP::3xFLAG::CSR-1 embryos at different stages (4-cell, 28-cell, 100-cell, 200-cell, and comma), shows that CSR-1 localizes to cytoplasmic granules in early embryos and is restricted to germ granules in late embryos. At least three individual embryos were imaged for each stage. Dotted white line marks perimeter of the embryo. Box marks germ granule localization of CSR-1. Scale bars, 5 μ m.

F. Box plot quantifying GFP::3xFLAG::CSR-1 granules at different embryonic stages. At least ten embryos at each stage were used for quantification. Each dot represents an individual embryo, and all data points are shown. Bolded midline indicates median value, box indicates the first and third quartiles, and whiskers represent the most extreme data points within 1.5 times the interquartile range. Lines connect the mean granule number (red dots) at each stage, illustrating the change in number of CSR-1 granules across embryonic development. Two-tailed t-tests were performed to determine statistical significance and p-values were adjusted for multiple comparisons. See Materials and Methods for a detailed description of quantification methods.

G. Live imaging of mCherry::EGO-1; GFP::3xFLAG::CSR-1 embryo at 28-cell stage, showing CSR-1 colocalization with EGO-1. At least ten individual embryos were imaged. Arrowheads point to examples of CSR-1 and EGO-1 colocalization at cytoplasmic granules. Scale bars, 5 μ m.

H. Live imaging of SIMR-1::mCherry::2xHA; GFP::3xFLAG::CSR-1 embryo at 28-cell stage, showing the absence of colocalization between SIMR-1 and CSR-1 with occasional adjacent localization. At least ten individual embryos were imaged. Arrowheads point to examples of SIMR-1 and CSR-1 granules that do not colocalize. Insets display examples of SIMR-1 and CSR-1 granules that are found adjacent to each other. Dotted white line marks perimeter of embryo. Scale bars, 5 μ m.

I. Model of CSR and SIMR granules in the somatic cells of *C. elegans* embryos. The RdRP EGO-1, which synthesizes CSR-class 22G-RNAs, localizes to CSR granules, where CSR-1 loading may take place. The RdRP RRF-1, along with RDE-3, ENRI-2, and unloaded NRDE-3 localize to SIMR granules. SIMR-1 and ENRI-2 recruits unloaded NRDE-3 to granule where RRF-1 may synthesize ERGO-dependent 22G-RNAs for loading into NRDE-3. After loading, NRDE-3 translocates to the nucleus and silences genes co-transcriptionally.

MUT-16 is the scaffolding protein for germline *Mutator* foci, thus we next investigated whether MUT-16 similarly scaffolds the cytoplasmic SIMR-1 granules in early embryos (Phillips et al. 2012 [↗](#)). We found that MUT-16 can be observed in cytoplasmic granules in the embryonic somatic cells (Supplementary Fig. 4I), similar to what has been observed in a previous study (Ouyang et al. 2019 [↗](#)), and both SIMR-1 and RDE-3 fail to assemble into cytoplasmic granules in the *mut-16* mutant (Fig. 4D [↗](#), Supplementary Fig. 4J). Notably, the germ granule association of SIMR-1 is unaffected, as SIMR-1 still localizes to germ granules at comma stage embryos and in the adult germline (Fig. 4D [↗](#)) (Manage et al. 2020 [↗](#)). Together, these data indicate that MUT-16 functions upstream of SIMR-1 and mediates the assembly of cytoplasmic granules in embryos. It is curious to note that, in a *mut-16* mutant where SIMR-1 association with cytoplasmic granules is lost in the somatic cells, SIMR-1 instead associates with mitotic spindles (Fig. 4D [↗](#)). To conclude, we have shown that the SIMR granules found in the somatic cells of early embryos contain the biogenesis machinery for WAGO-class 22G-RNAs, including RDE-3 and RRF-1, and depend on the scaffolding protein MUT-16 for assembly (Fig. 4I [↗](#)). The differential requirement for MUT-16 on the assembly of somatic SIMR-1 granules and the SIMR compartment of germ granules highlights a key difference between these two compartments, which have some parallel functions but distinct composition.

CSR-1 and EGO-1 associate with a distinct type of granule in early embryos

The Argonaute protein CSR-1 has also been previously seen at cytoplasmic granules in the soma of early embryos, a time at which CSR-1 is functioning to clear maternal-inherited mRNAs (Quarato et al. 2021 [↗](#); Seroussi et al. 2023 [↗](#); Ouyang et al. 2019 [↗](#)). Using a GFP-tagged CSR-1 strain we constructed previously (Nguyen and Phillips 2021 [↗](#)), we confirmed that CSR-1 forms prominent cytoplasmic granules in embryos visible prior to the 4-cell stage and present through 100-cell stage embryos, but disappear by the 200-cell stage, at which point only germ granule localization is visible (Fig. 4E [↗](#)). Quantification of the total number of CSR-1 granules per embryo across development shows that the CSR-1 granules are more abundant than the SIMR-1 and NRDE-3(HK-AA) granules and differ in the timing of their appearance and disappearance relative to SIMR-1 and NRDE-3(HK-AA) granules (Fig. 1C [↗](#), 2C [↗](#), 4F [↗](#)). Specifically, CSR-1 granules appear earlier and peak at the 28-cell stage, while SIMR-1 and NRDE-3(HK-AA) granules appear between 8- and 28-cell stages and peak at the 100-cell stage (Fig. 1C [↗](#), 2C [↗](#), 4F [↗](#)). The small RNAs bound by CSR-1 are synthesized by the RdRP, EGO-1, so we next assessed the localization of EGO-1 in early embryos. We found that EGO-1 colocalizes with CSR-1 in the somatic CSR-1 granules (Fig. 4G [↗](#)) and neither CSR-1 nor EGO-1 fully colocalizes with SIMR-1, although we occasionally observed adjacent localization between SIMR-1 and CSR-1 (Fig. 4H [↗](#), supplementary Fig. 4K). Lastly, unlike RRF-1 which requires SIMR-1 to localize to embryonic foci, EGO-1 localizes to cytoplasmic granules in the absence of *simr-1* (Fig. 4C [↗](#)). Together, our results show that the RdRPs, RRF-1 and EGO-1, localize to different cytoplasmic granules in the somatic cells of *C. elegans* embryos, where they colocalize with Argonaute proteins, NRDE-3 and CSR-1, respectively. Thus, we postulate that WAGO-class and CSR-class 22G-RNA biogenesis and loading are compartmentalized into cytoplasmic granules, differing from one another both spatially and temporally, in the somatic cells of early embryos (Fig. 4I [↗](#)).

NRDE-3 switches small RNA partners during embryonic development

The nuclear localization of NRDE-3 in the somatic cells of larvae depends on ERGO-1 and other proteins required for the biogenesis of ERGO-class 26G-RNAs (Guang et al. 2008 [↗](#)). Sequencing of NRDE-3-bound 22G-RNAs at the L4 to young adult transition identifies a set of endogenous targets that overlaps substantially with those of ERGO-1 (Seroussi et al. 2023 [↗](#)). Together, these data have led to the conclusion that NRDE-3 acts downstream of ERGO-1 to transcriptionally silence ERGO-target genes. Yet our data looking at the nuclear localization of NRDE-3 in embryos, demonstrate

that this model may be an incomplete picture. Specifically, in *eri-1* and *rde-3* mutants where 26G-RNA or WAGO-class 22G-RNA biogenesis are abolished, respectively, NRDE-3 remains localized to the nucleus in early embryos (**Fig. 2A** [↗](#)). The small RNA binding-defective NRDE-3(HK-AA) is localized exclusively to the cytoplasm at the same time point, indicating that small RNA binding is critical for nuclear import at this stage (**Fig. 2A** [↗](#)). Accordingly, we must postulate that NRDE-3 binds another class of small RNA to promote nuclear entry in very early embryos. To investigate the identity of NRDE-3-bound small RNAs across embryonic development and to explore the role of the SIMR-1 granules in promoting NRDE-3 small RNA binding, we immunoprecipitated NRDE-3 and sequenced associated small RNAs (IP-sRNA seq) in early embryos (≤ 100 -cell) and late embryos (≥ 300 -cell) in wild-type, *eri-1* mutant, *simr-1* mutant, and *enri-2* mutant animals (**Fig. 5A** [↗](#)).

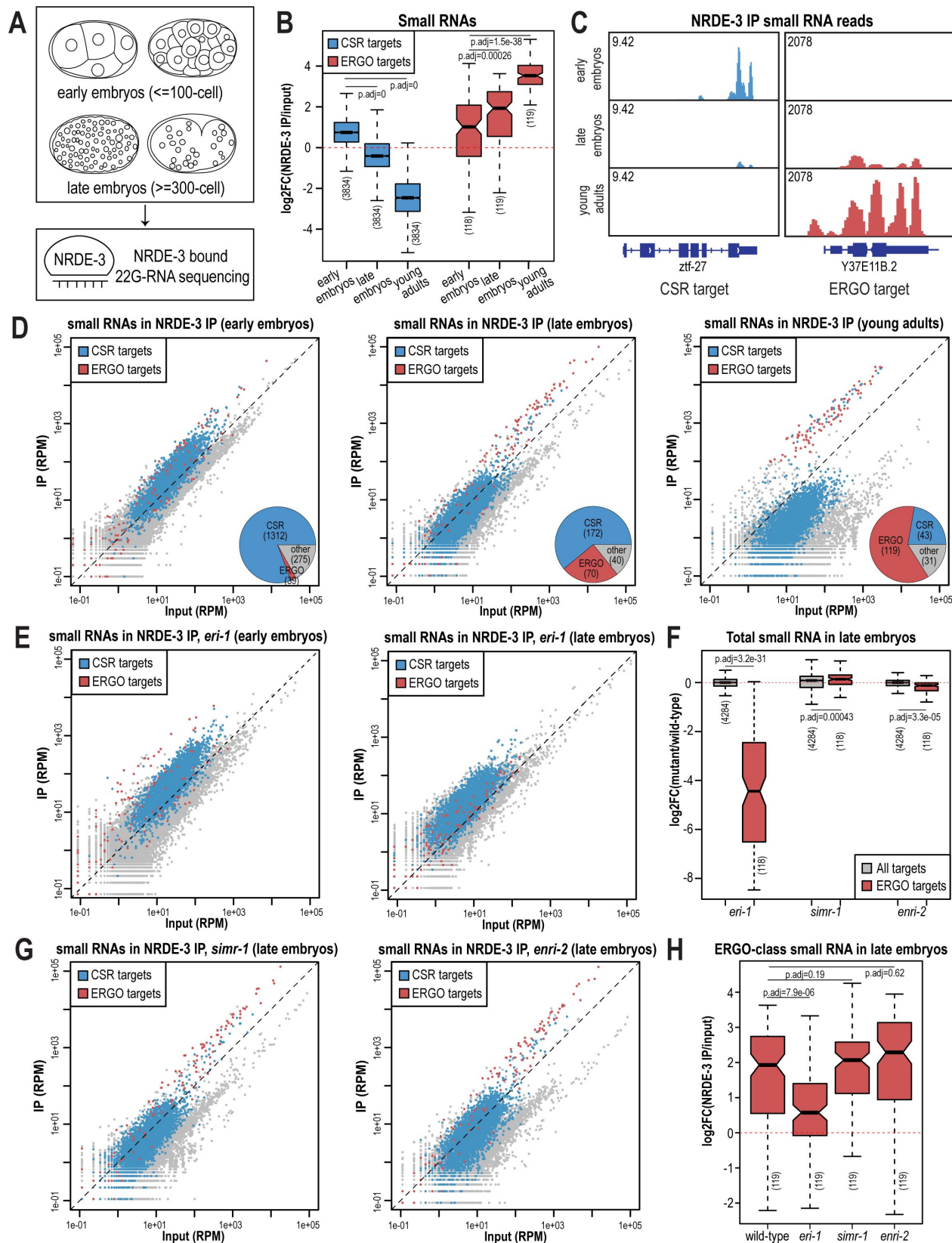


Figure 5.

NRDE-3 switches small RNA targets during development.

- A. Diagram of IP-sRNA seq on NRDE-3 early embryos (≤ 100 -cell stage) and late embryos (≥ 300 -cell). GFP::FLAG::NRDE-3 was immunoprecipitated from embryo lysate and its associated small RNAs were isolated for sequencing.
- B. Box plots depicting \log_2 (fold change small RNA abundance) in NRDE-3 IP compared to input for at least two biological replicates.
- C. Normalized NRDE-3-bound small RNA read distribution across a CSR-target gene (*ztf-27*) and an ERGO-target gene (Y37E11B.2) in early embryos, late embryos, and young adults. One representative replicate is shown.
- D. Normalized NRDE-3 IP compared to input small RNA reads in early embryos, late embryos, and young adults. CSR-target and ERGO-target genes are indicated in blue and red, respectively. One representative replicate is shown. Insets are pie charts describing numbers of CSR targets, ERGO targets, and other targets that are significantly enriched in the NRDE-3 IP. The enriched targets were defined as small RNAs with at least 2-fold enrichment in IP compared to input, average RPM > 10 , and p-values ≤ 0.05 .
- E. Normalized NRDE-3 IP compared to input small RNA reads in *eri-1* mutant early and late embryos. CSR-target and ERGO-target genes are indicated in blue and red, respectively. One representative replicate is shown.
- F. Box plots depicting \log_2 (fold change small RNA abundance) in mutants compared to wild-type in early embryos for two or three biological replicates.
- G. Normalized NRDE-3 IP compared to input small RNA reads in *simr-1* mutant and *enri-2* mutant late embryos. CSR-target and ERGO-target genes are indicated in blue and red, respectively. One representative replicate is shown.
- H. Box plots depicting \log_2 (fold change of ERGO-class small RNA abundance) in NRDE-3 IP compared to input in wild-type and mutants in late embryos for two or three biological replicates.

For box plots in B,F,H, bolded midline indicates median value, box indicates the first and third quartiles, and whiskers represent the most extreme data points within 1.5 times the interquartile range, excluding outliers. Two-tailed t-tests were performed to determine statistical significance and p-values were adjusted for multiple comparisons.

Prior to analyzing our data, we sought to better define the expected NRDE-3-bound small RNAs. We initially planned to use two previously defined ERGO-target gene lists: the first list (ERGO - Manage) is defined by small RNAs significantly depleted at least two-fold in *ergo-1* mutant compared to wild-type at the gravid adult stage, with at least 10 reads per million (RPM) in wild-type samples and a DESeq2 adjusted p-value of < 0.05 (Manage et al. 2020 [\[1\]](#)); the second list (ERGO - Fischer) is defined by genes reduced by 67% in *eri-7* adults or an average of 67% in *ergo-1*, *eri-1*, *eri-6*, and *eri-7* embryos, with at least 10 RPM in wild-type (Fischer et al. 2011 [\[2\]](#)). However, small RNAs targeting many of these previously defined ERGO targets were not enriched by NRDE-3 in a published NRDE-3 IP-sRNA seq data on young adult animals that have begun oogenesis but do not yet have embryos (Seroussi et al. 2023 [\[3\]](#)) (Supplementary Fig. 5A,B). To define a more stringent NRDE-3-target gene list at the young adult stage, we chose genes with at least four-fold enrichment ($\log_2 \text{FC} \geq 2$) and 100 RPM (RPM ≥ 100) from the NRDE-3 IP-sRNA seq in young adults (Seroussi et al. 2023 [\[3\]](#)). This new list contains 119 genes and largely overlaps with the two previously defined ERGO-target gene lists (Supplementary Fig. 5C,D). To further confirm that this newly defined gene list represents NRDE-3 targets, we analyzed published small RNA and mRNA sequencing data from wild-type and *nrde-3* mutant mixed-stage embryos (before the bean stage) (Padeken et al. 2021 [\[4\]](#)).

Compared to the Manage and Fischer ERGO-target gene lists, the NRDE-3-target gene list shows more significant small RNA depletion and a greater increase in mRNA expression in the *nrde-3* mutant compared to wild-type (Supplementary Fig. 5A-C,E,F). Therefore, we use the new NRDE-3-target gene list to represent the ERGO-1 pathway-dependent, NRDE-3-target genes (referred to here as ERGO targets) in the rest of this study (Supplementary Table 4).

We next examined the small RNAs bound to NRDE-3 in wild-type early embryos and late embryos, comparing our data to the published NRDE-3 IP-sRNA seq data on young adult animals (Seroussi et al. 2023 [\[1\]](#)). Strikingly, we found that in early embryos, the majority of small RNAs bound by NRDE-3 are CSR-class 22G-RNAs, which become progressively less enriched as the animals develop into late embryos and then young adults (Fig. 5B-D [\[1\]](#)). In contrast, enrichment for small RNAs targeting ERGO-target genes increases as *C. elegans* develops, and they become the majority of NRDE-3-bound small RNAs by young adulthood (Fig. 5B-D [\[1\]](#)). NRDE-3 also binds to CSR-target genes in the early embryos of the *eri-1* mutant, when it is observed to localize to the nucleus, indicating that the production of these NRDE-3-bound CSR-class 22G-RNAs is independent of *eri-1* and that CSR-class 22G-RNAs are likely sufficient to promote nuclear entry of NRDE-3 in the early embryo (Fig. 2A [\[1\]](#), 5E). To conclude, NRDE-3 binds to CSR-class 22G-RNA in early embryos but switches to bind preferentially to ERGO-dependent 22G-RNA in late embryos and young adults, suggesting that NRDE-3 may have two separable functions at distinct developmental time points. It is also curious to note that the change in small RNA preference of NRDE-3 coincides with the appearance and disappearance of the cytoplasmic SIMR granules, suggesting a role for SIMR-1 and ENRI-2 in promoting the loading of NRDE-3 with ERGO-dependent 22G-RNAs.

SIMR-1 and ENRI-2 are not absolutely required to promote NRDE-3 small RNA specificity

Since ERGO-dependent 22G-RNA loading was mainly observed in late embryos, we focused on NRDE-3-bound small RNAs in the *eri-1* mutant, *simr-1* mutant, and *enri-2* mutant late embryos to determine the role of SIMR-1 granules in promoting NRDE-3 small RNA binding specificity. We first examined the levels of ERGO-dependent small RNAs in the total small RNA samples and observed depletion of small RNAs mapping to ERGO-target genes in the *eri-1* mutant (Fig. 5E,F [\[1\]](#)). This result is consistent with previous research indicating that ERI-1 is required for ERGO-class 26G RNA production and downstream ERGO-dependent 22G-RNA production (Vasale et al. 2010 [\[2\]](#); Han et al. 2009 [\[3\]](#); Guang et al. 2008 [\[4\]](#)). ERGO-dependent small RNAs are not substantially depleted in *simr-1* or *enri-2* mutants, indicating that RRF-1 can still synthesize a similar amount of ERGO-dependent 22G-RNAs when the cytoplasmic SIMR granules are absent (Fig. 5F,G [\[1\]](#)). Following NRDE-3 immunoprecipitation, we similarly observed a reduction in NRDE-3 binding to ERGO-dependent small RNAs in the *eri-1* mutant while no significant reduction in NRDE-3 binding to ERGO-dependent small RNAs was observed in either *simr-1* or *enri-2* mutants (Fig. 5G,H [\[1\]](#)). These results indicate that SIMR-1 and ENRI-2 are not absolutely required for the production of the ERGO-dependent small RNAs during embryogenesis and the loading of these small RNAs into NRDE-3. Nonetheless, since unloaded NRDE-3 and the small RNA biogenesis machinery RRF-1 are dispersed to the cytoplasm in the *simr-1* mutant (Fig. 3A [\[1\]](#), 4C [\[1\]](#)), NRDE-3 may still be able to load the ERGO-dependent 22G-RNAs synthesized by RRF-1 but perhaps with lower efficiency.

NRDE-3 binds to CSR-class 22G-RNAs in germ cells and early embryos

Our foregoing results show that NRDE-3 localizes to the nucleus in early embryos independent of ERGO-dependent 22G-RNAs and binds to CSR-class 22G-RNA at this developmental stage (Fig. 2A [\[1\]](#), Fig. 5B-E [\[1\]](#)). Interestingly, in late embryos from *eri-1* mutant and *rde-3* mutant, we have observed nuclear localization of NRDE-3 only in the primordial germ cells (Fig. 2A [\[1\]](#)), raising an intriguing hypothesis that NRDE-3 might bind to CSR-class 22G-RNAs in germ cells throughout development and inherit NRDE-3-bound CSR-class 22G-RNAs to early embryos.

To test this hypothesis, we first asked whether the nuclear localization of NRDE-3 in the adult germline depends on ERI-1 and RDE-3. We found that NRDE-3 localizes to the nuclei of pachytene germ cells and oocytes in wild-type, *eri-1* mutants, and *rde-3* mutants, but is restricted to the cytoplasm in *nrde-3(HK-AA)* small RNA binding mutants, consistent with our observations of NRDE-3 localization in early embryos (**Fig. 6A** [↗](#)). Next, to confirm that NRDE-3 binds to CSR-class 22G-RNAs in germ cells and early embryos, we utilized auxin-inducible degron (AID) system to deplete the RdRP EGO-1 by growing the worms on 4mM auxin plates starting at the L1 stage (Zhang et al. 2015 [↗](#)) (supplementary Fig. 6A). Surprisingly, NRDE-3 still localizes to nuclei in both germ cells and early embryos upon EGO-1 depletion (supplementary Fig. 6B), indicating that NRDE-3 either does not exclusively bind CSR-class 22G-RNAs in the germline, or NRDE-3 has the capacity to bind other small RNAs when the CSR-class 22G-RNAs are absent. We did observe some NRDE-3 localization to cytoplasmic granules in a subset of 8-cell stage embryos following EGO-1 depletion (supplementary Fig. 6B), suggesting that a proportion of NRDE-3 might be unloaded. To further probe which small RNAs NRDE-3 binds to in the germline, we introduced a *rde-3* mutation into the GFP::NRDE-3; degron::EGO-1 strain to deplete WAGO-class 22G-RNAs. We observed that NRDE-3 no longer localizes to the nucleus in both germline and early embryos in the absence of both WAGO-class 22G-RNAs and CSR-class 22G-RNAs (**Fig. 6B** [↗](#)). These results, in combination with our sequencing data, indicate that NRDE-3 likely binds CSR-class 22G-RNAs in the germline and early embryos but has the capacity to additionally bind WAGO-class 22G-RNAs when CSR-class 22G-RNAs are depleted. Furthermore, because somatic transcription is thought to initiate around the 4-cell stage (Seydoux and Fire 1994 [↗](#)), the correlation of NRDE-3 localization between oocytes and early embryos suggests that NRDE-3, loaded with CSR-class 22G-RNAs, is likely inherited by the early embryo from the parental germline.

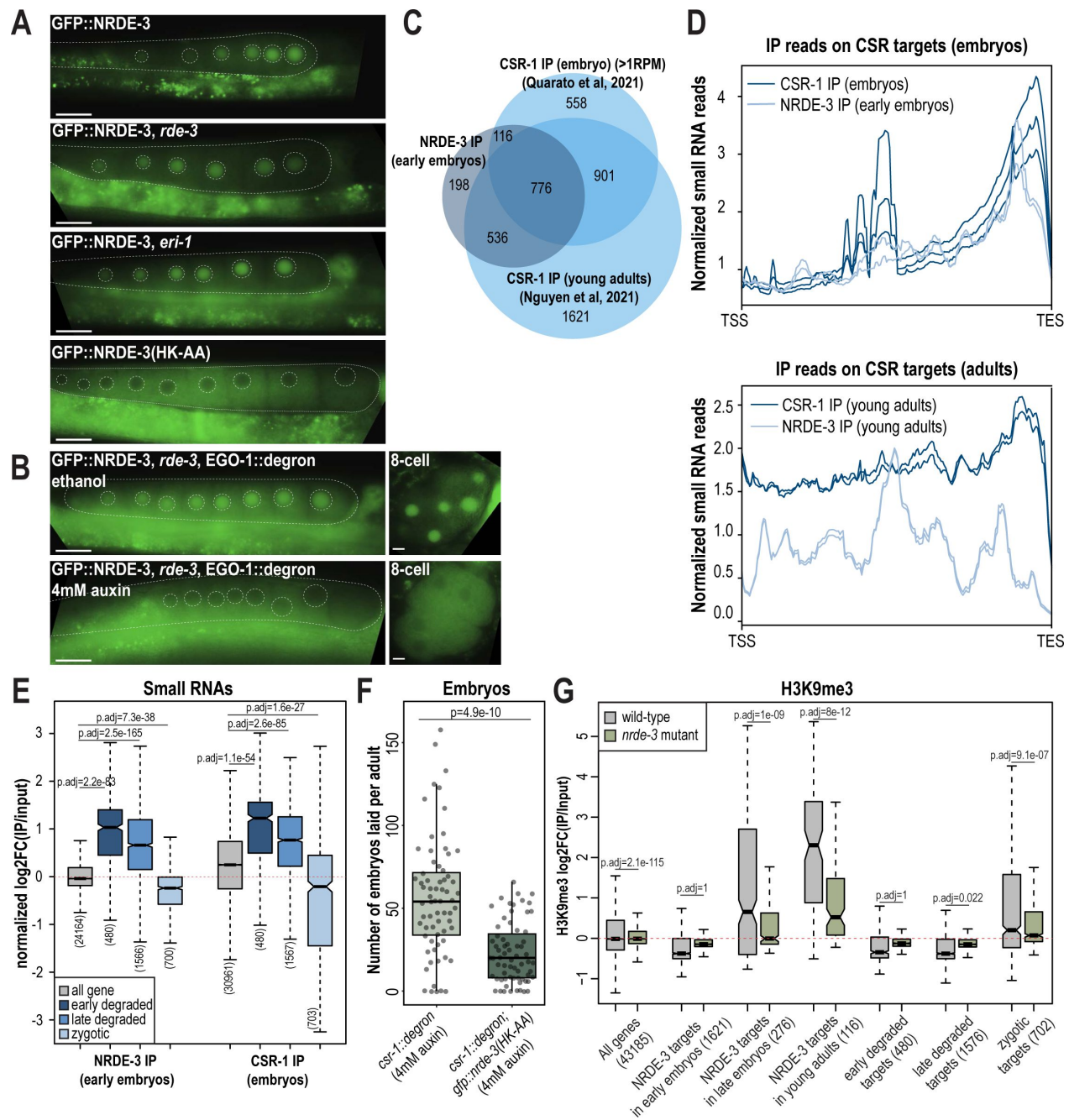


Figure 6.

NRDE-3 associates with CSR-class 22G-RNA in early embryos.

A. Live imaging of GFP::3xFLAG::NRDE-3 in one-day-adult germlines for wild-type, *eri-1*, *rde-3*, and *nrde-3(HK-AA)* mutants, showing that NRDE-3 localizes to the nuclei of oocytes in wild-type, *eri-1* mutant, and *rde-3* mutants, and to the cytoplasm in the *nrde-3(HK-AA)* mutant. At least five individual gonads were imaged for each genotype. Dotted white line traces the proximal portion of the *C. elegans* gonad and outlines the individual oocytes. Scale bars, 25 μ m.

B. Live imaging of one-day-adult germlines and 8-cell embryos for *degron::EGO-1*; GFP::3xFLAG::NRDE-3 in a *rde-3* mutant with ethanol (top) and 4mM auxin (bottom) treatment, showing that loss of both WAGO-class and CSR-class 22G-RNAs (*rde-3* mutant and *degron*-mediated EGO-1 depletion) leads to cytoplasmic localization of NRDE-3 in both oocytes and early embryos. At least five individual gonads and embryos were imaged for each treatment condition. Dotted white line traces the proximal portion of the *C. elegans* gonad and outlines the individual oocytes. Scale bars, 25 μ m in adults and 5 μ m in embryos.

C. Venn diagrams indicate overlap of NRDE-3 IP enriched targets in early embryos (this work), CSR-1 IP enriched targets in young adults (Nguyen *et al.*, 2021), and CSR-1 IP enriched targets in embryos (Quarato *et al.*, 2021 [DOI](#)).

D. Density plot of small RNA enrichment on CSR targets in CSR-1 IP (dark blue), NRDE-3 IP (light blue) in embryos (top) and adults (bottom). Transcription start site (TSS) to transcription end site (TES) were plotted using normalized small RNA reads. All replicates are shown as individual lines.

E. Box plots depicting normalized \log_2 (fold change of small RNA abundance in IP vs input) in a NRDE-3 IP in early embryos and CSR IP in embryos for two or three biological replicates. All genes list includes all genes expressed in IP or input. Early degraded mRNAs are maternal mRNAs that show at least twofold reduction in mRNA levels in early embryos (4 to 20 cell-stage) compared to 1-cell embryos (Quarato *et al.*, 2021 [DOI](#)). Late degraded mRNAs are maternal mRNAs that show stable levels of mRNAs in early embryos and at least twofold reduction in late embryos (more than 20-cell stage) (Quarato *et al.*, 2021 [DOI](#)). Zygotic mRNAs are mRNAs that are not detectable in 1-cell embryos but accumulate in early and late embryos (Quarato *et al.*, 2021 [DOI](#)).

F. Box plot quantifying the number of embryos laid per adult *csr-1::degron* or *csr::degron*, *gfp::nrde-3(HK-AA)* animal on 4mM auxin plate. At least 65 individuals from each strain were scored. Each dot represents an individual animal, and all data points are shown.

G. Box plot depicting \log_2 (fold change of H3K9me3 level in IP vs input) in wild-type (grey) and *nrde-3* mutant (green) mixed-stage embryos, indicating that the H3K9me3 level of NRDE-3 targets in early embryos are not affected in *nrde-3* mutant. Anti-H3K9me3 ChIP-seq data was obtained from Padeken *et al.* (2021) [DOI](#).

For box plots in E,F,G, bolded midline indicates median value, box indicates the first and third quartiles, and whiskers represent the most extreme data points within 1.5 times the interquartile range, excluding outliers. Two-tailed t-tests were performed to determine statistical significance and p-values were adjusted for multiple comparisons.

We next sought to assess the degree to which NRDE-3-bound 22G-RNAs are similar to CSR-1-bound 22G-RNAs in early embryos. First, we examined the overlap of NRDE-3-targeted genes in early embryos with CSR-1-targeted genes in embryos or young adult animals. We found that the genes targeted by NRDE-3 substantially overlap with CSR-target genes at both stages (**Fig. 6C** [DOI](#)) (Quarato *et al.* 2021 [DOI](#); Nguyen and Phillips 2021 [DOI](#)). Furthermore, the CSR-target genes yielding the highest abundance of CSR-1-bound small RNAs in embryos also have the highest abundance of NRDE-3-bound small RNAs (Supplementary Fig. 6C). These CSR-target genes with highly abundant CSR-bound small RNAs are highly enriched by NRDE-3 only in embryos and not in young adults (Supplementary Fig. 6C). Next, CSR-class 22G-RNAs tend to be enriched at the 3' ends of mRNAs

while WAGO-class 22G-RNAs are more evenly distributed across the gene bodies in adult animals (Ishidate et al. 2018 [DOI](#); Singh et al. 2021 [DOI](#)). Comparing NRDE-3-bound small RNAs from early embryos to a published dataset of CSR-1-bound small RNA from mixed-stage embryos, we found that both NRDE-3 and CSR-1 are heavily enriched for small RNAs derived from the 3' ends of CSR-target genes in embryos (**Fig. 6D** [DOI](#)). Interestingly, in adult animals, CSR-1-bound 22G-RNAs are still enriched for small RNA derived from the 3' end of CSR-target genes, however there is additionally a much higher enrichment of small RNAs derived from the gene bodies compared to in embryos (**Fig. 6D** [DOI](#)). It has previously been proposed that two types of CSR-class 22G-RNAs exist, those that depend on CSR-1 catalytic activity for their production and are derived primarily from target gene bodies, and those that are produced independently of CSR-1 catalytic activity and are derived primarily from target 3'UTRs (Singh et al. 2021 [DOI](#)). Our data points to both NRDE-3 and CSR-1 binding only the latter, CSR-1 catalytic activity-independent, type of CSR-class 22G-RNA in early embryos. In contrast, NRDE-3 does not show enrichment for small RNAs derived from the 3' ends of ERGO target genes in embryos, and rather the small RNAs are distributed more evenly across the gene bodies (Supplementary Fig. 6D). CSR-1 utilizes its catalytic activity to slice and clear maternally-inherited mRNAs from early embryos, preferentially binding to transcripts degraded early in embryogenesis (Quarato et al. 2021 [DOI](#)). We further demonstrate that NRDE-3 similarly binds preferentially to early-degraded transcripts, suggesting it may be functioning in parallel to CSR-1 (**Fig. 6E** [DOI](#)). Lastly, the expression of mRNAs targeted by CSR-1 decreases across embryonic development as CSR-1 actively slices and clears these maternal transcripts (Quarato et al. 2021 [DOI](#)). We similarly find that the mRNAs targeted by NRDE-3 in young embryos, which correspond primarily to CSR-target mRNAs, decrease in expression across development, while its targets in young adults, corresponding primarily to ERGO-target mRNAs, increase in expression across development (supplementary Fig. 6E). Together, these data reveal that NRDE-3 binds to the same group of small RNAs as CSR-1 in early embryos, and may work hand-in-hand with CSR-1 to repress transcripts of maternal origin.

To further investigate whether NRDE-3 and CSR-1 function synergistically, we examined the fertility of the *csr-1::degron* strain and the *csr-1::degron; gfp::nrde-3(HK-AA)* strain upon auxin treatment to deplete CSR-1. As expected, both strains had 100% viable progeny with ethanol control treatment (supplementary Fig. 6F). When growing on 4mM auxin plates, the number of embryos laid by the *csr-1::degron; gfp::nrde-3(HK-AA)* double mutant was significantly lower compared to the *csr-1::degron* single mutant and more of the double mutant produced no embryos (11.9%) compared to the *csr-1::degron* single mutant strain (7.5%), indicating a more severe sterility defect in the *csr-1::degron; nrde-3(HK-AA)* double mutant compared to the *csr-1::degron* alone (**Fig. 6F** [DOI](#), supplementary Fig. 6F). Additionally, 5.9% of the auxin-treated *csr-1::degron* animals produced some F1 progeny that hatched, compared to no F1 hatching for any of the auxin-treated *csr-1::degron; gfp::nrde-3(HK-AA)* double mutant animals (supplementary Fig. 6F). All together, these results indicate that loss of NRDE-3 enhances the fertility defects of CSR-1 and suggest that NRDE-3 and CSR-1 function synergistically for early embryonic development.

NRDE-3 is a nuclear Argonaute protein that recruits histone methyltransferases to target genes to deposit histone modifications such as H3K9me3 and H3K27me3 at these loci (Guang et al. 2008 [DOI](#); Burton et al. 2011 [DOI](#); Mao et al. 2015 [DOI](#)). To examine whether NRDE-3 promotes deposition of H3K9me3 at CSR-target genes during embryogenesis, we analyzed the published anti-H3K9me3 ChIP-seq data of wild-type and *nrde-3* mutant mixed-staged embryos (Padeken et al. 2021 [DOI](#)). In wild-type embryos, the targets of NRDE-3 in young adults, which correspond to ERGO-target genes, have high H3K9me3 levels, and are significantly decreased in the *nrde-3* mutant (**Fig. 6G** [DOI](#)). These data are consistent with previous research demonstrating that NRDE-3 deposits H3K9me3 at ERGO target genes (Burton et al. 2011 [DOI](#)). However, NRDE-3 targets in early embryos do not show H3K9me3 enrichment in wild-type and do not have a significant change in the *nrde-3* mutant (**Fig. 6G** [DOI](#)). The same trend is also observed in the early degraded and late degraded targets (**Fig. 6G** [DOI](#)). These results indicate that the CSR targets are not H3K9 trimethylated in the early embryos.

However, we cannot rule out the possibility that NRDE-3 may function to deposit other histone modification targets such as H3K27me3 or inhibit RNA pol II on CSR targets to transcriptionally silence these genes in early embryos.

Discussion

Germ granules are phase-separated condensates that localize to the perinuclear region of germ cells. In *C. elegans*, the known constituents of the germ granule have expanded over the last decades, such that germ granules now comprise multiple domains including P granules, *Mutator* foci, Z granules, and SIMR foci. Here we discovered that several components of SIMR foci and *Mutator* foci also localize to cytoplasmic granules during specific stages of embryogenesis. We propose that these granules serve as sites for the synthesis and loading of 22G-RNAs into the nuclear Argonaute NRDE-3. Furthermore, we showed that NRDE-3 switches its small RNA targets during embryogenesis, coincident with the formation of SIMR granules. Together, our study reveals a new world of embryonic RNAi factor condensates and uncovers two temporally distinct roles for NRDE-3, underscoring the need for careful examination of localization and targets of RNAi pathways across development (**Fig. 7A** [↗](#)).

A role for SIMR-1 as a platform for nuclear Argonaute protein loading

Previously we demonstrated that SIMR-1 and HRDE-2 are required to recruit unloaded HRDE-1, the germline nuclear Argonaute protein, to germ granules and to ensure correct 22G-RNA loading ([Chen and Phillips 2024](#) [↗](#)). Here we reveal that SIMR-1 and another HRDE-2 paralog, ENRI-2, are similarly essential to recruit unloaded NRDE-3, the somatic nuclear Argonaute protein, to embryonic SIMR granules. We speculate that SIMR-1 and ENRI-2 are similarly important for NRDE-3 22G-RNA loading; however, we did not observe a significant change in the small RNAs loaded by NRDE-3 in *simr-1* or *enri-2* mutant embryos. While initially surprising based on the results of similar experiments with HRDE-1 in the germline, we envision several possible explanations. First, it is possible that SIMR-1 and ENRI-2 act to bring unloaded NRDE-3 in close proximity to the ERGO-dependent 22G-RNA biogenesis machinery, but that NRDE-3 loading can still occur diffusely in the cytoplasm, albeit with lower efficiency. In addition, both the RdRP RRF-1 and unloaded NRDE-3 diffusely localize to cytoplasm in the *simr-1* mutant (**Fig. 3A** [↗](#), 4C), suggesting that NRDE-3 may load the ERGO-class small RNAs synthesized in the cytoplasm in the absence of SIMR-1. Differences in NRDE-3 loading efficiency would likely not be detected by our NRDE-3 IP-small RNA sequencing experiment. Second, SIMR-1 and ENRI-2 could act to sequester unloaded NRDE-3 away from other small RNAs (i.e. CSR-class 22G-RNAs) to prevent misloading. Misloading should be detectable in our NRDE-3 IP-small RNA sequencing experiment; however, it is unclear the extent to which newly synthesized, and unloaded CSR-class 22G-RNAs are even present in the cytoplasm, as the primary source for CSR-class 22G-RNAs may be the maternal germline. Thus, unlike in the adult germline where HRDE-1 incorrectly loads CSR-class 22G-RNAs in the absence of HRDE-2, there may not be an equivalent source of incorrect small RNAs that NRDE-3 can bind to (i.e. correct length, 5' nucleotide and modifications) in the embryo. To further probe these possibilities, we need to more carefully assess the dynamics of NRDE-3 loading across embryonic development and possibly disrupt the formation of embryonic CSR granules to determine whether compartmentalization of the CSR-class 22G-RNA pathway is also contributing to correct loading of NRDE-3 in the absence of SIMR-1 and ENRI-2.

We do not know the precise functions of SIMR-1 and ENRI-2, however we have previously proposed that SIMR-1 mediates protein-protein interactions through its extended Tudor domain ([Manage et al. 2020](#) [↗](#)). ENRI-2 and its paralog HRDE-2 have structural similarities to a HELIC domain, and SIMR-1, ENRI-2, and HRDE-2 have large unstructured domains (Supplementary Fig.

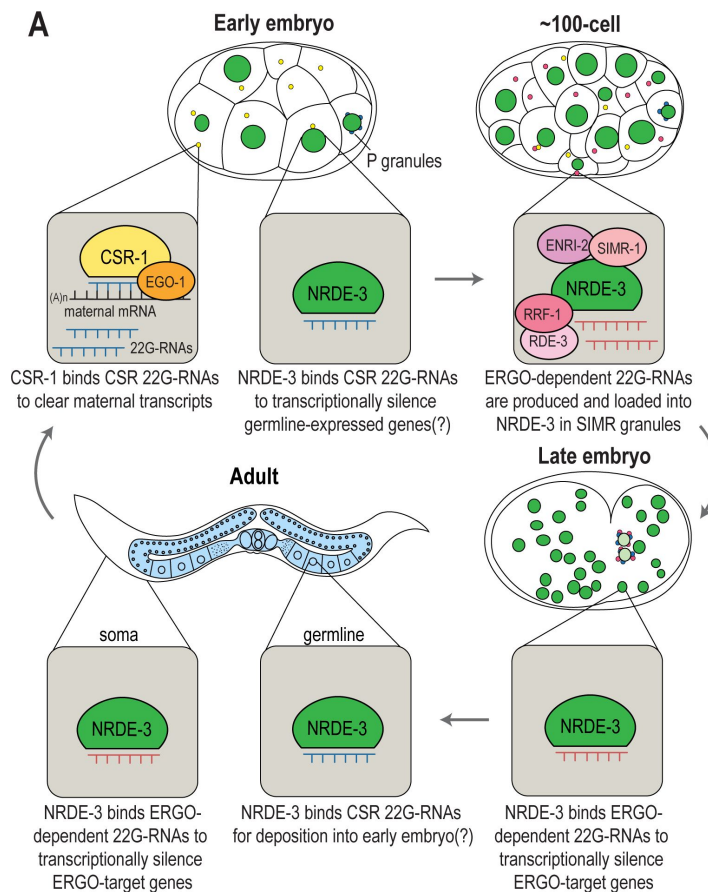


Figure 7.

Model of the function of cytoplasmic granules in *C. elegans* development.

Model of NRDE-3, SIMR-1, and CSR-1 function during *C. elegans* development. In early embryos, CSR-1 and EGO-1 localize to CSR granules and synthesize CSR 22G-RNAs to slice and clear maternal mRNAs. NRDE-3 binds CSR 22G-RNA in the nucleus and may transcriptionally silence germline-expressed genes. During mid-embryogenesis (e.g. around the 100-cell stage), unloaded NRDE-3, ENRI-2, RRF-1, and RDE-3 are recruited to SIMR granules in somatic cells by SIMR-1, where ERGO-dependent 22G-RNAs are produced and loaded to NRDE-3. In late embryos, NRDE-3 binds ERGO-dependent 22G-RNAs and silences ERGO-target genes in the nucleus. In adult *C. elegans*, somatic localized NRDE-3 associates with ERGO-dependent 22G-RNAs to transcriptionally silence ERGO-target genes, while germline localized NRDE-3 associates with CSR-class 22G-RNAs, possibly for deposition into early embryos.

7A) (Lewis et al. 2020 [↗](#); Chen and Phillips 2024 [↗](#)). With the advent of protein complex prediction algorithms (Abramson et al. 2024 [↗](#)), we sought to examine the potential physical interactions between ENRI-2 and NRDE-3, as well as their paralogs HRDE-2 and HRDE-1. In both models, the structured HELICc domain of HRDE-2 and ENRI-2 dock on the Mid domain of their respective Argonaute partners. Interestingly, the unstructured C-terminal domains of ENRI-2 and HRDE-2 extend into the small RNA binding pocket of their respective nuclear Argonaute binding partners (Supplementary Fig. 7B). At this point, we do not know whether these structures are reflective of the actual geometry of the proteins *in vivo*, but it is tempting to speculate that the C-terminal disordered regions of the ENRI-2/HRDE-2 proteins could regulate 22G-RNA loading through interaction with the small RNA binding pocket of NRDE-3 and HRDE-1. Further study will be necessary to determine whether these interactions between disordered regions and the small RNA binding pocket are necessary for correct small RNA loading and whether that mechanism extends to other WAGO proteins.

Compartmentalization of RNAi pathways

Most of the studies on the organization of *C. elegans* RNAi factors in granules focus on the germline. Here we find that multiple proteins associated with 22G-RNA biogenesis and function, including SIMR-1, RDE-3, RRF-1, ENRI-2, and unloaded NRDE-3, are localized distinct condensates in *C. elegans* embryos. We speculate that these SIMR granules, which appear and then disappear during the course of embryonic development, play a functional role in the NRDE-3 nuclear RNAi pathway. This idea leads to an intriguing question: what role does organization of the RNAi pathways into condensates play in the soma vs. in the germline?

In germ cells, RNAi factors are visibly segregated into distinct compartments within the germ granule which assemble hierarchically (Uebel et al. 2023 [↗](#)). Germ granules are also intimately linked to nuclear pores, leading to a model where highly concentrated mRNAs, newly exported from and adjacent to the nuclear pore, nucleate assembly of regulatory factors into visible granules. In fact, nuclear pores are clustered beneath germ granules in germ cells, and evidence suggests that most, if not all, nascent mRNAs are exported through pores associated with germ granules (Pitt et al. 2000 [↗](#); Sheth et al. 2010 [↗](#)). In contrast, nuclear pores are distributed more evenly across the nuclear periphery in embryos and, in this work, we find that while some embryonic SIMR granules appear adjacent to the nuclear periphery, many are distributed in the cytoplasm (see **Fig. 2A** [↗](#), for example). Thus, unlike in germ granules, there is no obvious trajectory from the nucleus that RNAs would follow to end up in embryonic SIMR granules. Further, in the germline, we have speculated that the adjacent and hierarchical assembly of germ granule compartments could be determined by the order of molecular events required for RNA silencing (Uebel et al. 2023 [↗](#)). While we on occasion see docking between embryonic SIMR granules and CSR granules (**Fig. 4H** [↗](#)), we do not see any more complex arrangement of granule compartments in embryos similar to what we have observed in the germline. What that means regarding the functionality of embryonic SIMR granules is unclear. Another possibility worth considering is that SIMR granules are not actually required for ERGO-dependent 22G-RNA biogenesis and NRDE-3 loading in embryos but rather that they reflect a concentration of the small RNA biogenesis machinery beyond the solubility limit of the cytoplasm, resulting in the demixing of some RNP complexes into visible SIMR granules (Putnam et al. 2023 [↗](#)). By this “incidental condensate” model, ERGO-dependent 22G-RNA biogenesis and NRDE-3 loading occur just as efficiently, or perhaps more so, diffusely in the cytoplasm.

Both embryonic and germ granules exhibit dynamic expression patterns, suggesting that expression and function of small RNA factors are critical at discrete developmental time points. In the germline, multiple Argonaute proteins are expressed exclusively during oogenesis (ERGO-1) or spermatogenesis (ALG-3, ALG-4, CSR-1b, WAGO-10) (Billi et al. 2012 [↗](#); Han et al. 2009 [↗](#); Conine et al. 2010 [↗](#); Reinke et al. 2004 [↗](#); Nguyen and Phillips 2021 [↗](#); Charlesworth et al. 2021 [↗](#)) and MUT-16 expression fluctuates across germ cell development, peaking in the mitotic region (Uebel et al. 2020 [↗](#)). Similarly, embryonic SIMR granules appear in early embryos and disappear by late

embryogenesis. Regardless as to whether SIMR granules are incidental condensates or functional sites for NRDE-3 loading, these data indicate that the levels or activities of these proteins are developmentally regulated.

It is additionally curious that embryonic and germ granules share many protein components yet possess distinct differences in content and assembly requirements. For instance, several RNAi proteins, such as RRF-1 and RDE-3, are shared between *Mutator* foci and embryonic SIMR granules, while the paralogous ENRI-2/NRDE-3 and HRDE-2/HRDE-1 pairs are found in embryonic SIMR granules and germline SIMR foci, respectively. It is unclear why the *Mutator* and SIMR components are visible as separate compartments in germ granules but are together in embryonic SIMR foci. This difference is highlighted by the requirement for MUT-16 in the assembly of embryonic SIMR granules but not germline SIMR foci (**Fig. 4D**) (Manage et al. 2020). Further investigation into the assembly and protein components of embryonic and germ granules will be crucial for elucidating the functional differences between embryonic and germ granules and dissecting the mechanisms of 22G-RNA loading into NRDE-3.

The small RNA plasticity of NRDE-3

Argonautes are conventionally known to bind small RNAs with high specificity. In this study, we unveil the remarkable versatility of the nuclear Argonaute NRDE-3, demonstrating its ability to bind multiple classes of small RNAs and exhibit distinct functions throughout development. Argonaute proteins with the capacity to bind multiple types or classes of small RNAs have been observed in other organisms. For example, both siRNAs and miRNAs can be loaded into the four human Argonautes (Ago1-4) and both siRNAs and miRNAs can guide Ago2-dependent target cleavage (Meister et al. 2004; Liu et al. 2004). Our discovery is somewhat different, however, in that NRDE-3 binds its two preferred classes of small RNAs, CSR-class 22G-RNAs and ERGO-dependent 22G-RNAs, at distinct developmental stages, indicating that there must be a switch from one class of small RNA to the other during embryogenesis. Interestingly, a more recent study in the parasitic nematode *Acaris* revealed that the *Acaris* paralog of NRDE-3, AsNRDE-3, exhibits a dramatic change in associated small RNAs during spermatogenesis, targeting repetitive sequences and transposons in early stages of spermatogenesis and mRNAs in late meiosis (Zagoskin et al. 2022). Curiously, the mRNAs targeted by AsNRDE-3 in late meiosis largely overlap with the targets of AsCSR-1, the *Ascaris* paralog of CSR-1, and it is proposed that AsNRDE-3 could act in concert with AsCSR-1 at the late stages of meiosis to clear spermatogenic and meiotic mRNAs from the developing spermatids (Zagoskin et al. 2022). These data further suggest that the ability of NRDE-3 to target both repetitive sequences and germline-expressed genes at distinct developmental timepoints may be a conserved feature of this protein. It is currently unknown how this small RNA switching is achieved. It is possible that there is an active mechanism to unload the CSR-class 22G-RNAs and replace them with ERGO-dependent 22G-RNAs, or to degrade NRDE-3 loaded with CSR-class 22G-RNAs. However, we prefer the simpler model where NRDE-3 loaded with CSR-class 22G-RNAs, initially deposited into embryo from the maternal germline, are diluted out as the animal develops. Newly synthesized NRDE-3 in the embryo is loaded with ERGO-dependent 22G-RNAs to execute the small RNA “switch.” The idea that Argonaute proteins can be utilized at distinct timepoints with different small RNA partners to create multi-functionality is intriguing, especially in the vein of rapidly clearing transcripts from a cell to engineer a new developmental program. Achieving higher resolution small RNA-Argonaute interactions with tissue- and developmental-specific staging will be crucial to fully elucidate the roles of Argonaute proteins during development in *C. elegans* and other organisms.

In summary, this work investigating the role of SIMR granules in embryos, together with our previous study of SIMR foci in the germline (Chen and Phillips 2024), has identified a new mechanism for small RNA loading of nuclear Argonaute proteins in *C. elegans*. The two paralogous proteins, HRDE-2 and ENRI-2, recruit unloaded nuclear Argonautes HRDE-1 and NRDE-3 to small RNA production centers organized by SIMR-1, where loading can occur. These small RNA loading sites are essential in the germline to promote small RNA binding specificity, however they may

also contribute to efficiency and specificity of small RNA loading in embryos. We further discovered an intriguing repository of cytoplasmic granules during embryogenesis that do not exhibit the same organization or hierarchical assembly as germ granules, highlighting the importance of further investigation into the relationship between RNA silencing pathways and RNA granules during embryogenesis. Lastly, we observed a striking phenomenon where the NRDE-3 nuclear Argonaute protein possesses the ability to switch small RNA binding partners, presumably altering mRNA targets and function, during development. Together, these findings reveal that the precise regulation of small RNA pathway components through diverse mechanisms, such as spatial-temporal separation and hierarchical physical interactions, is crucial for accurate gene regulation and developmental transitions in *C. elegans*.

Materials and methods

C. elegans stains

C. elegans strains were maintained at 20°C on NGM plates seeded with OP50 *E. coli* according to standard conditions unless otherwise stated (Brenner 1974 [DOI](#)). All strains used in this project are listed in Supplementary Table 1.

CRISPR-mediated strain construction

For *nrde-3(cmp324[HK-AA])*, *enri-1(cmp328)*, *enri-2(cmp318)*, and *rde-3/mut-2(cmp337)*, we used an oligo repair template and RNA guide. For *enri-1(cmp320[enri-1::mCherry::2xHA])*, we used an RNA guide and PCR amplified repair template (Supplementary Table 2). For injections using a single gene-specific crRNA, the injection mix included 0.25 µg/µl Cas9 protein (IDT), 100 ng/µl tracrRNA (IDT), 14 ng/µl dpy-10 crRNA, 42 ng/µl gene-specific crRNA, and 110 ng/µl of the oligo repair template. For injections using two gene-specific crRNAs, the injection mix included 0.25 µg/µl Cas9 protein (IDT), 100 ng/µl tracrRNA (IDT), 14 ng/µl dpy-10 crRNA, 21 ng/µl each gene-specific crRNA, and 110 ng/µl of each repair template.

The following strains were used for injection: *enri-2(cmp318)* and *enri-1(cmp320[enri-1::mCherry::2xHA])* into wild-type N2 strain. *nrde-3(cmp324[HK-AA])* and *enri-1(cmp328)* into JMC237: *nrde-3(tor131[GFP::3xFLAG::nrde-3])* X. *rde-3/mut-2(cmp337)* into USC1615: *ego-1(cmp317[ego-1::degron])* I; *ieSi38 [Psun-1::TIR1::mRuby::sun-1 3' UTR]* IV; *nrde-3(tor131[GFP::3xFLAG::nrde-3])* X. Following injection, F1 animals with the Rol phenotype were isolated and genotyped by PCR to identify heterozygous animals with the mutations of interest, then F2 animals were further singled out to identify homozygous mutant animals.

Live imaging

Live imaging of *C. elegans* embryos was performed in M9 buffer. Young embryos were obtained by dissecting gravid adult *C. elegans*, and old embryos were obtained by manually picking embryos laid on the NGM plate. Live imaging of *C. elegans* adult germline was performed in M9 buffer containing sodium azide to prevent movement. Day-one-adult *C. elegans* were obtained by manually picking L4s and leaving L4s at 20°C for about 24 hours. Imaging was performed on a DeltaVision Elite microscope (GE Healthcare) using a 60x N.A. 1.42 oil-immersion objective. Images were pseudocolored using Adobe Photoshop.

Granule number quantification

Granule number quantification was performed in FIJI/ImageJ2 (version 2.9.0). At least 10 embryos were imaged on a DeltaVision Elite microscope with 37 optical sections of a total 22.20µm sample thickness from the bottom of the sample. Images were deconvolved to eliminate backgrounds. Z

stacks were opened using the 3D object counter plugin for FIJI, and the granule counting threshold for each image was manually adjusted to obtain the least background and most granules.

Western blot

Synchronized adult *C. elegans* were harvested (~72 h at 20 °C after L1 arrest) and 200 adults were loaded per lane. Proteins were resolved on 4–12% Bis-Tris polyacrylamide gels (Thermo Fisher, NW04122BOX), transferred to nitrocellulose membranes (Thermo Fisher, LC2001), and probed with rat anti-HA-peroxidase 1:1000 (Roche 12013819001) or mouse anti-actin 1:10,000 (Abcam ab3280). Secondary HRP antibodies were purchased from Thermo Fisher. Unedited western blots are provided in the Source Data File.

Small RNA library preparation and sequencing

For *C. elegans* embryo staging and collection, synchronized arrested L1s were grown on enriched peptone plates at 17°C until the young adult stage. Adult *C. elegans* stage was monitored carefully under DeltaVision microscope by live imaging. For early embryo collection (<=100-cell), adult animals were washed off from plates with H₂O and bleached as soon as the first animals had 1–4 eggs (around 68–70 hours depending on the strain and the incubator temperature). For late embryo collection (>=300-cell), adult animals were washed off from plates with H₂O and bleached when about half of the worms had 1–6 eggs (~70–72 hours depending on the strain and the incubator temperature). After bleaching, embryos were washed twice with M9 buffer, and filtered through 40µm cell strainers (Fisherbrand™ Sterile Cell Strainers, 40µm) twice to clear the residual worm body. To reach >=300-cell stage for late embryo collection, embryos were additionally incubated in M9 buffer at 20°C for 4.5 hours. Then embryos were washed once with IP buffer (50 mM Tris-Cl pH 7.5, 100 mM KCl, 2.5 mM MgCl₂, 0.1% Nonidet P40 substitute) containing Protease Inhibitor (Thermo Fisher A32965). Embryos were kept on ice during washes to prevent further development. 500,000 embryos were collected for each replicate. Following washes, embryos were flash-frozen by placing tubes in a container with ethanol and dry ice. A small aliquot of embryos was examined on the Deltavision microscope to confirm the developmental stage immediately before freezing. Frozen embryos were stored at –80°C until immunoprecipitation.

For immunoprecipitation followed by small RNA sequencing in embryos, ~500,000 synchronized embryos were sonicated with Fisher Sonifier 550 with a microtip (15s on, 45s off, 10% power, total 2 minutes on time). After sonication, insoluble particulate was removed by centrifugation at 21,000g for 30 minutes. Immunoprecipitation was performed using anti-FLAG Affinity Matrix (Sigma Aldrich, A2220). NRDE-3-bound RNAs were isolated using TRIzol reagent (Thermo Fisher, 15596018), followed by chloroform extraction and isopropanol precipitation. Small RNAs (18 to 30-nt) were size selected on homemade 10% Urea-polyacrylamide gels from total RNA samples. Small RNAs were treated with 5' RNA polyphosphatase (Epicenter RP8092H) and ligated to 3' pre-adenylated adapters with Truncated T4 RNA ligase (NEB M0373L). Small RNAs were then hybridized to the reverse transcription primer, ligated to the 5' adapter with T4 RNA ligase (NEB M0204L), and reverse transcribed with Superscript III (Thermo Fisher 18080-051). Small RNA libraries were amplified using Q5 High-Fidelity DNA polymerase (NEB M0491L) and size selected on a homemade 10% polyacrylamide gel. Library concentration was determined using the Qubit 1X dsDNA HS Assay kit (Thermo Fisher Q33231) and quality was assessed using the Agilent BioAnalyzer. Libraries were sequenced on the Illumina NextSeq2000 (SE 75-bp reads) platform. Primer sequences are available in Supplementary Table2. Differentially expressed gene lists and gene lists used in this paper can be found in Supplementary Table3. Sequencing library statistics summary can be found in Supplementary Table4.

Bioinformatic analysis

For small RNA libraries, sequences were parsed from adapters and quality filtered using FASTX-Toolkit (version 0.0.13) (Greg Hannon 2010 [↗](#)). Filtered reads were mapped to the *C. elegans* genome, WS258, using Bowtie2 (version 2.5.0) (Langmead and Salzberg 2012 [↗](#)). Mapped reads were assigned to genomic features using featureCounts which is part of the Subread package (version 2.0.1) (Liao et al. 2014 [↗](#)). Differential expression analysis was performed using edgeR (3.40.2) (Robinson et al. 2010 [↗](#)). To define gene lists from IP experiments, a twofold-change cutoff, an edgeR adjusted p-value of ≤ 0.05 , and at least 10 RPM in the IP libraries were required to identify genes with significant changes in small RNA levels.

Data Availability

The RNA sequencing data generated in this study are available through Gene Expression Omnibus (GEO) under accession code GSE273239. Source data file is provided with this paper.

Acknowledgements

We thank the members of the Phillips lab for helpful discussions and feedback on the manuscript, and the labs of Julie Claycomb, John Kim, Heng-Chi Lee, and Mihail Sarov for generously providing strains. This work was supported by the National Institute of Health grant R35 GM119656 (to CMP). Some strains were provided by the CGC, which is funded by NIH Office of Research Infrastructure Programs (P40 OD010440). Next generation sequencing was performed by the USC Molecular Genomics Core, which is supported by award number P30 CA014089 from the National Cancer Institute.

Author contributions

S.C.: Conceptualization, Investigation, Formal analysis, Writing—original draft, Writing—reviewing and editing, Visualization C.M.P.: Conceptualization, Formal Analysis, Writing—original draft, Writing—reviewing and editing, Supervision, Funding Acquisition.

Competing interests

The authors declare no competing interests.

References

- Abramson J *et al.* (2024) **Accurate structure prediction of biomolecular interactions with AlphaFold 3** *Nature* **630**:493–500
- Aoki K, Moriguchi H, Yoshioka T, Okawa K, Tabara H (2007) **In vitro analyses of the production and activity of secondary small interfering RNAs in *C. elegans*** *EMBO J* **26**:5007–5019
- Ashe A, BÉlicard T, Le Pen J, Sarkies P, Frézal L, Lehrbach NJ, Félix M-A, Miska EA. (2013) **A deletion polymorphism in the *Caenorhabditis elegans* RIG-I homolog disables viral RNA dicing and antiviral immunity** *eLife* **2**
- Billi AC, Alessi AF, Khivansara V, Han T, Freeberg M, Mitani S, Kim JK (2012) **The *Caenorhabditis elegans* HEN1 Ortholog, HENN-1, Methylates and Stabilizes Select Subclasses of Germline Small RNAs** *PLOS Genet* **8**
- Brangwynne CP, Eckmann CR, Courson DS, Rybarska A, Hoege C, Gharakhani J, Jülicher F, Hyman AA (2009) **Germline P Granules Are Liquid Droplets That Localize by Controlled Dissolution/Condensation** *Science* **324**:1729–1732
- Brenner S (1974) **THE GENETICS OF CAENORHABDITIS ELEGANS** *Genetics* **77**:71–94
- Buck AH, Blaxter M (2013) **Functional diversification of Argonautes in nematodes: an expanding universe** *Biochem Soc Trans* **41**:881–886
- Buckley BA, Burkhart KB, Gu SG, Spracklin G, Kershner A, Fritz H, Kimble J, Fire A, Kennedy S (2012) **A nuclear Argonaute promotes multigenerational epigenetic inheritance and germline immortality** *Nature* **489**:447–451
- Burton NO, Burkhart KB, Kennedy S (2011) **Nuclear RNAi maintains heritable gene silencing in *Caenorhabditis elegans*** *Proc Natl Acad Sci* **108**:19683–19688
- Charlesworth AG *et al.* (2021) **Two isoforms of the essential *C. elegans* Argonaute CSR-1 differentially regulate sperm and oocyte fertility** *Nucleic Acids Res* **49**:8836–8865
- Chen C-CG, Simard MJ, Tabara H, Brownell DR, McCollough JA, Mello CC (2005) **A Member of the Polymerase β Nucleotidyltransferase Superfamily Is Required for RNA Interference in *C. elegans*** *Curr Biol* **15**:378–383
- Chen S, Phillips CM (2024) **HRDE-2 drives small RNA specificity for the nuclear Argonaute protein HRDE-1** *Nat Commun* **15**
- Claycomb JM *et al.* (2009) **The Argonaute CSR-1 and Its 22G-RNA Cofactors Are Required for Holocentric Chromosome Segregation** *Cell* **139**:123–134
- Conine CC, Batista PJ, Gu W, Claycomb JM, Chaves DA, Shirayama M, Mello CC (2010) **Argonautes ALG-3 and ALG-4 are required for spermatogenesis-specific 26G-RNAs and thermotolerant sperm in *Caenorhabditis elegans*** *Proc Natl Acad Sci* **107**:3588–3593

- Ding S-W, Li H, Lu R, Li F, Li W-X (2004) **RNA silencing: a conserved antiviral immunity of plants and animals** *Virus Res* **102**:109–115
- Du Z, Shi K, Brown JS, He T, Wu W-S, Zhang Y, Lee H-C, Zhang D. (2023) **Condensate cooperativity underlies transgenerational gene silencing**
- Félix M-A *et al.* (2011) **Natural and Experimental Infection of Caenorhabditis Nematodes by Novel Viruses Related to Nodaviruses** *PLOS Biol* **9**
- Fire A, Xu S, Montgomery MK, Kostas SA, Driver SE, Mello CC (1998) **Potent and specific genetic interference by double-stranded RNA in Caenorhabditis elegans** *Nature* **391**:806–811
- Fischer SEJ, Montgomery TA, Zhang C, Fahlgren N, Breen PC, Hwang A, Sullivan CM, Carrington JC, Ruvkun G (2011) **The ERI-6/7 Helicase Acts at the First Stage of an siRNA Amplification Pathway That Targets Recent Gene Duplications** *PLOS Genet* **7**
- Gallo CM, Munro E, Rasoloson D, Merritt C, Seydoux G (2008) **Processing bodies and germ granules are distinct RNA granules that interact in C. elegans embryos** *Dev Biol* **323**:76–87
- Gent JI, Lamm AT, Pavelec DM, Maniar JM, Parameswaran P, Tao L, Kennedy S, Fire AZ (2010) **Distinct Phases of siRNA Synthesis in an Endogenous RNAi Pathway in C. elegans Soma** *Mol Cell* **37**:679–689
- Greg Hannon (2010) **Greg Hannon. 2010. FASTX-Toolkit: FASTQ/a short-reads pre-processing tools.** http://hannonlab.cshl.edu/fastx_toolkit/.
- Gu W *et al.* (2009) **Distinct Argonaute-Mediated 22G-RNA Pathways Direct Genome Surveillance in the C. elegans Germline** *Mol Cell* **36**:231–244
- Guang S, Bochner AF, Pavelec DM, Burkhart KB, Harding S, Lachowiec J, Kennedy S (2008) **An Argonaute Transports siRNAs from the Cytoplasm to the Nucleus** *Science* **321**:537–541
- Han T, Manoharan AP, Harkins TT, Bouffard P, Fitzpatrick C, Chu DS, Thierry-Mieg D, Thierry-Mieg J, Kim JK (2009) **26G endo-siRNAs regulate spermatogenic and zygotic gene expression in Caenorhabditis elegans** *Proc Natl Acad Sci* **106**:18674–18679
- Han W, Sundaram P, Kenjale H, Grantham J, Timmons L (2008) **The Caenorhabditis elegans rsd-2 and rsd-6 Genes Are Required for Chromosome Functions During Exposure to Unfavorable Environments** *Genetics* **178**:1875–1893
- Höck J, Meister G (2008) **The Argonaute protein family** *Genome Biol* **9**
- Ishidate T, Ozturk AR, Durning DJ, Sharma R, Shen E, Chen H, Seth M, Shirayama M, Mello CC (2018) **ZNFX-1 Functions within Perinuclear Nuage to Balance Epigenetic Signals** *Mol Cell* **70**:639–649
- Langmead B, Salzberg SL (2012) **Fast gapped-read alignment with Bowtie 2** *Nat Methods* **9**:357–359
- Lewis A *et al.* (2020) **A Family of Argonaute-Interacting Proteins Gates Nuclear RNAi** *Mol Cell* **78**:862–875

- Liao Y, Smyth GK, Shi W (2014) **featureCounts: an efficient general purpose program for assigning sequence reads to genomic features** *Bioinformatics* **30**:923–930
- Liu J, Carmell MA, Rivas FV, Marsden CG, Thomson JM, Song J-J, Hammond SM, Joshua-Tor L, Hannon GJ (2004) **Argonaute2 Is the Catalytic Engine of Mammalian RNAi** *Science* **305**:1437–1441
- Ma J-B, Yuan Y-R, Meister G, Pei Y, Tuschl T, Patel DJ (2005) **Structural basis for 5'-end-specific recognition of guide RNA by the A. fulgidus Piwi protein** *Nature* **434**:666–670
- Manage KI *et al.* (2020) **A tudor domain protein, SIMR-1, promotes siRNA production at piRNA-targeted mRNAs in C. elegans** *eLife* **9**
- Mao H, Zhu C, Zong D, Weng C, Yang X, Huang H, Liu D, Feng X, Guang S (2015) **The Nrde Pathway Mediates Small-RNA-Directed Histone H3 Lysine 27 Trimethylation in Caenorhabditis elegans** *Curr Biol* **25**:2398–2403
- McEwan DL, Weisman AS, Hunter CP (2012) **Uptake of Extracellular Double-Stranded RNA by SID-2** *Mol Cell* **47**:746–754
- Meister G, Landthaler M, Patkaniowska A, Dorsett Y, Teng G, Tuschl T (2004) **Human Argonaute2 Mediates RNA Cleavage Targeted by miRNAs and siRNAs** *Mol Cell* **15**:185–197
- Nguyen DAH, Phillips CM (2021) **Arginine methylation promotes siRNA-binding specificity for a spermatogenesis-specific isoform of the Argonaute protein CSR-1** *Nat Commun* **12**
- Ouyang JPT, Folkmann A, Bernard L, Lee C-Y, Seroussi U, Charlesworth AG, Claycomb JM, Seydoux G (2019) **P Granules Protect RNA Interference Genes from Silencing by piRNAs** *Dev Cell* **50**:716–728
- Padeken J, Methot S, Zeller P, Delaney CE, Kalck V, Gasser SM (2021) **Argonaute NRDE-3 and MBT domain protein LIN-61 redundantly recruit an H3K9me3 HMT to prevent embryonic lethality and transposon expression** *Genes Dev* **35**:82–101
- Pak J, Fire A (2007) **Distinct Populations of Primary and Secondary Effectors During RNAi in C. elegans** *Science* **315**:241–244
- Parker R, Sheth U (2007) **P Bodies and the Control of mRNA Translation and Degradation** *Mol Cell* **25**:635–646
- Phillips CM *et al.* (2014) **MUT-14 and SMUT-1 DEAD Box RNA Helicases Have Overlapping Roles in Germline RNAi and Endogenous siRNA Formation** *Curr Biol* **24**:839–844
- Phillips CM, Montgomery TA, Breen PC, Ruvkun G (2012) **MUT-16 promotes formation of perinuclear Mutator foci required for RNA silencing in the C. elegans germline** *Genes Dev* **26**:1433–1444
- Pitt JN, Schisa JA, Priess JR (2000) **P Granules in the Germ Cells of Caenorhabditis elegans Adults Are Associated with Clusters of Nuclear Pores and Contain RNA** *Dev Biol* **219**:315–333
- Putnam A, Thomas L, Seydoux G (2023) **RNA granules: functional compartments or incidental condensates?** *Genes Dev* **37**:354–376

- Quarato P, Singh M, Cornes E, Li B, Bourdon L, Mueller F, Didier C, Cecere G (2021) **Germline inherited small RNAs facilitate the clearance of untranslated maternal mRNAs in *C. elegans* embryos** *Nat Commun* **12**
- Reinke V, Gil IS, Ward S, Kazmer K (2004) **Genome-wide germline-enriched and sex-biased expression profiles in *Caenorhabditis elegans*** *Development* **131**:311–323
- Robinson MD, McCarthy DJ, Smyth GK (2010) **edgeR: a Bioconductor package for differential expression analysis of digital gene expression data** *Bioinformatics* **26**:139–140
- Sakaguchi A *et al.* (2014) ***Caenorhabditis elegans* RSD-2 and RSD-6 promote germ cell immortality by maintaining small interfering RNA populations** *Proc Natl Acad Sci* **111**:E4323–E4331
- Sarkies P, Miska EA (2013) **RNAi pathways in the recognition of foreign RNA: antiviral responses and host–parasite interactions in nematodes** *Biochem Soc Trans* **41**:876–880
- Seroussi U, Li C, Sundby AE, Lee TL, Claycomb JM, Saltzman AL (2022) **Mechanisms of epigenetic regulation by *C. elegans* nuclear RNA interference pathways** *Semin Cell Dev Biol* **127**:142–154
- Seroussi U, Lugowski A, Wadi L, Lao RX, Willis AR, Zhao W, Sundby AE, Charlesworth AG, Reinke AW, Claycomb JM. (2023) **A comprehensive survey of *C. elegans* argonaute proteins reveals organism-wide gene regulatory networks and functions** *eLife* **12**
- Seydoux G, Dunn MA (1997) **Transcriptionally repressed germ cells lack a subpopulation of phosphorylated RNA polymerase II in early embryos of *Caenorhabditis elegans* and *Drosophila melanogaster*** *Development* **124**:2191–2201
- Seydoux G, Fire A (1994) **Soma-germline asymmetry in the distributions of embryonic RNAs in *Caenorhabditis elegans*** *Development* **120**:2823–2834
- Sheth U, Pitt J, Dennis S, Priess JR (2010) **Perinuclear P granules are the principal sites of mRNA export in adult *C. elegans* germ cells** *Development* **137**:1305–1314
- Shirayama M, Stanney W, Gu W, Seth M, Mello CC (2014) **The Vasa Homolog RDE-12 Engages Target mRNA and Multiple Argonaute Proteins to Promote RNAi in *C. elegans*** *Curr Biol* **24**:845–851
- Shukla A, Yan J, Pagano DJ, Dodson AE, Fei Y, Gorham J, Seidman JG, Wickens M, Kennedy S (2020) **. poly(UG)-tailed RNAs in genome protection and epigenetic inheritance** *Nature* **582**:283–288
- Sijen T, Fleenor J, Simmer F, Thijssen KL, Parrish S, Timmons L, Plasterk RHA, Fire A (2001) **On the Role of RNA Amplification in dsRNA-Triggered Gene Silencing** *Cell* **107**:465–476
- Singh M, Cornes E, Li B, Quarato P, Bourdon L, Dingli F, Loew D, Proccacia S, Cecere G (2021) **Translation and codon usage regulate Argonaute slicer activity to trigger small RNA biogenesis** *Nat Commun* **12**
- Spracklin G, Fields B, Wan G, Becker D, Wallig A, Shukla A, Kennedy S (2017) **The RNAi Inheritance Machinery of *Caenorhabditis elegans*** *Genetics* **206**:1403–1416

- Tijsterman M, May RC, Simmer F, Okihara KL, Plasterk RHA (2004) **Genes Required for Systemic RNA Interference in *Caenorhabditis elegans*** *Curr Biol* **14**:111–116
- Uebel CJ, Agbede D, Wallis DC, Phillips CM (2020) **Mutator Foci Are Regulated by Developmental Stage, RNA, and the Germline Cell Cycle in *Caenorhabditis elegans*** *G3 GenesGenomesGenetics* **10**:3719–3728
- Uebel CJ, Manage KI, Phillips CM. (2021) **SIMR foci are found in the progenitor germ cells of *C. elegans* embryos**
- Uebel CJ, Rajeev S, Phillips CM (2023) ***Caenorhabditis elegans* germ granules are present in distinct configurations and assemble in a hierarchical manner** *Dev Camb Engl* **150**
- Udipke D, Strome S (2010) **P Granule Assembly and Function in *Caenorhabditis elegans*** *Germ Cells J Androl* **31**:53–60
- Vasale JJ, Gu W, Thivierge C, Batista PJ, Claycomb JM, Youngman EM, Duchaine TF, Mello CC, Conte D (2010) **Sequential rounds of RNA-dependent RNA transcription drive endogenous small-RNA biogenesis in the ERGO-1/Argonaute pathway** *Proc Natl Acad Sci* **107**:3582–3587
- Wan G, Fields BD, Spracklin G, Shukla A, Phillips CM, Kennedy S (2018) **Spatiotemporal regulation of liquid-like condensates in epigenetic inheritance** *Nature* **557**:679–683
- Wang JT, Seydoux G, Germ Cell Development in *C. elegans*, Schedl T. (2013) **Germ Cell Specification** *Advances in Experimental Medicine and Biology* New York: Springer :17–39 https://doi.org/10.1007/978-1-4614-4015-4_2
- Winston WM, Sutherlin M, Wright AJ, Feinberg EH, Hunter CP (2007) ***Caenorhabditis elegans* SID-2 is required for environmental RNA interference** *Proc Natl Acad Sci* **104**:10565–10570
- Yang H, Vallandingham J, Shiu P, Li H, Hunter CP, Mak HY (2014) **The DEAD Box Helicase RDE-12 Promotes Amplification of RNAi in Cytoplasmic Foci in *C. elegans*** *Curr Biol* **24**:832–838
- Yigit E, Batista PJ, Bei Y, Pang KM, Chen C-CG, Tolia NH, Joshua-Tor L, Mitani S, Simard MJ, Mello CC (2006) **Analysis of the *C. elegans* Argonaute Family Reveals that Distinct Argonautes Act Sequentially during RNAi** *Cell* **127**:747–757
- Zagoskin MV, Wang J, Neff AT, Veronezi GMB, Davis RE (2022) **Small RNA pathways in the nematode *Ascaris* in the absence of piRNAs** *Nat Commun* **13**
- Zhang C, Montgomery TA, Fischer SEJ, Garcia SMDA, Riedel CG, Fahlgren N, Sullivan CM, Carrington JC, Ruvkun G (2012) **The *Caenorhabditis elegans* RDE-10/RDE-11 Complex Regulates RNAi by Promoting Secondary siRNA Amplification** *Curr Biol* **22**:881–890
- Zhang L, Ward JD, Cheng Z, Dernburg AF (2015) **The auxin-inducible degradation (AID) system enables versatile conditional protein depletion in *C. elegans*** *Development* **142**:4374–4384

Editors

Reviewing Editor

Marcelo Mori

State University of Campinas, Campinas, Brazil

Senior Editor

David Ron

University of Cambridge, Cambridge, United Kingdom

Reviewer #1 (Public review):

Summary:

Chen and Phillips describe the dynamic appearance of cytoplasmic granules during embryogenesis analogous to SIMR germ granules, and distinct from CSR-1-containing granules, in the *C. elegans* germline. They show that the nuclear Argonaute NRDE-3, when mutated to abrogate small RNA binding, or in specific genetic mutants, partially colocalizes to these granules along with other RNAi factors, such as SIMR-1, ENRI-2, RDE-3, and RRF-1. Furthermore, NRDE-3 RIP-seq analysis in early vs. late embryos is used to conclude that NRDE-3 binds CSR-1-dependent 22G RNAs in early embryos and ERGO-1-dependent 22G RNAs in late embryos. These data lead to their model that NRDE-3 undergoes small RNA substrate "switching" that occurs in these embryonic SIMR granules and functions to silence two distinct sets of target transcripts - maternal, CSR-1 targeted mRNAs in early embryos and duplicated genes and repeat elements in late embryos.

Strengths:

The identification and function of small RNA-related granules during embryogenesis is a poorly understood area and this study will provide the impetus for future studies on the identification and potential functional compartmentalization of small RNA pathways and machinery during embryogenesis.

Weaknesses:

(1) While the authors acknowledge the following issue, their finding that loss of SIMR granules has no apparent impact on NRDE-3 small RNA loading puts the functional relevance of these structures into question. As they note in their Discussion, it is entirely possible that these embryonic granules may be "incidental condensates." It would be very welcomed if the authors could include some evidence that these SIMR granules have some function; for example, does the loss of these SIMR granules have an effect on CSR-1 targets in early embryos and ERGO-1-dependent targets in late embryos?

(2) The analysis of small RNA class "switching" requires some clarification. The authors re-define ERGO-1-dependent targets in this study to arrive at a very limited set of genes and their justification for doing this is not convincing. What happens if the published set of ERGO-1 targets is used? Further, the NRDE-3 RIP-seq data is used to conclude that NRDE-3 predominantly binds CSR-1 class 22G RNAs in early embryos, while ERGO-1-dependent 22G RNAs are enriched in late embryos. a) The relative ratios of each class of small RNAs are given in terms of unique targets. What is the total abundance of sequenced reads of each class in the NRDE-3 IPs? b) The "switching" model is problematic given that even in late embryos, the majority of 22G RNAs bound by NRDE-3 is in the CSR-1 class (Figure 5D). c) A major difference between NRDE-3 small RNA binding in *eri-1* and *simr-1* mutants appears to be that NRDE-3 robustly binds CSR-122G RNAs in *eri-1* but not in *simr-1* in late embryos. This result should be better discussed.

(3) Ultimately, if the switching is functionally important, then its impact should be observed in the expression of their targets. RNA-seq or RT-qPCR of select CSR-1 and ERGO-1 targets should be assessed in *nrde-3* mutants during early vs late embryogenesis.

<https://doi.org/10.7554/eLife.102226.1.sa2>

Reviewer #2 (Public review):

Summary:

NRDE-3 is a nuclear WAGO-clade Argonaute that, in somatic cells, binds small RNAs amplified in response to the ERGO-class 26G RNAs that target repetitive sequences. This manuscript reports that, in the germline and early embryos, NRDE-3 interacts with a different set of small RNAs that target mRNAs. This class of small RNAs was previously shown to bind to a different WAGO-clade Argonaute called CSR-1, which is cytoplasmic, unlike nuclear NRDE-3. The switch in NRDE-3 specificity parallels recent findings in *Ascaris* where the *Ascaris* NRDE homolog was shown to switch from sRNAs that target repetitive sequences to CSR-class sRNAs that target mRNAs.

The manuscript also correlates the change in NRDE-3 specificity with the appearance in embryos of cytoplasmic condensates that accumulate SIMR-1, a scaffolding protein that the authors previously implicated in sRNA loading for a different nuclear Argonaute HRDE-1. By analogy, and through a set of correlative evidence, the authors argue that SIMR foci arise in embryogenesis to facilitate the change in NRDE-3 small RNA repertoire. The paper presents lots of data that beautifully documents the appearance and composition of the embryonic SIMR-1 foci, including evidence that a mutated NRDE-3 that cannot bind sRNAs accumulates in SIMR-1 foci in a SIMR-1-dependent fashion.

Weaknesses:

The genetic evidence, however, does not support a requirement for SIMR-1 foci: the authors detected no defect in NRDE-3 sRNA loading in *simr-1* mutants. Although the authors acknowledge this negative result in the discussion, they still argue for a model (Figure 7) that is not supported by genetic data. My main suggestion is that the authors give equal consideration to other models - see below for specifics.

<https://doi.org/10.7554/eLife.102226.1.sa1>

Reviewer #3 (Public review):

Summary:

Chen and Phillips present intriguing work that extends our view on the *C. elegans* small RNA network significantly. While the precise findings are rather *C. elegans* specific there are also messages for the broader field, most notably the switching of small RNA populations bound to an argonaute, and RNA granules behavior depending on developmental stage. The work also starts to shed more light on the still poorly understood role of the CSR-1 argonaute protein and supports its role in the decay of maternal transcripts. Overall, the work is of excellent quality, and the messages have a significant impact.

Strengths:

Compelling evidence for major shift in activities of an argonaute protein during development, and implications for how small RNAs affect early development. Very balanced

and thoughtful discussion.

Weaknesses:

Claims on col-localization of specific 'granules' are not well supported by quantitative data.

<https://doi.org/10.7554/eLife.102226.1.sa0>